Integrated design of system structure and delayed resonator towards efficient non-collocated vibration absorption

Adam Peichl[a], Matěj Kuře[a], Wim Michiels[b], Tomáš Vyhlídal[a]

[a]*Department of Instrumentation and Control Engineering, Faculty of Mechanical Engineering, Czech Technical University in Prague, Technická 4, 166 07 Prague 6, Czechia,*
[b]*Department of Computer Science, KU Leuven, Celestijnenlaan 200A, B-3001 Heverlee, Belgium,*

Abstract

The problem of non-collocated vibration absorption by a delayed resonator is addressed with emphasis on system fatigue resistance and energy efficiency of control actions. The analysis is performed for a system consisting of an arbitrary large series of flexibly linked single-degree-of-freedom masses. For the stage where the vibration of the target mass is fully absorbed by the non-collocated resonator, key forces, motion amplitudes and potential energies across the system structure are assessed. Next, a complete parameter set of the resonator gain and delay is derived, and the actuation force and power needed by the resonator for the full vibration absorption is determined. The derived quantities are utilized in forming an optimization problem to balance minimal risk of fatigue across the system structure and power needed by the resonator, under the closed loop stability and parameter constraints. Next to the gain and delay of the resonator, selected structural parameters of the system are used as variables in the constrained nonlinear optimization problem. Experimental and numerical case studies are included to demonstrate benefits of the proposed integrated structural and control design.

Keywords: Non-collocated vibration absorption, Delayed resonator, Structural analysis, Constrained optimization, Fatigue, Energy efficiency.

1. Introduction

Vibration absorbers have become established tools to mitigate adverse effects of vibration in a wide range of engineering applications. Traditionally, the vibration absorber is deployed

at the place of the mechanical structure, where vibrations are to be suppressed. This setting will further be referred to as *collocated vibration absorption*. The collocated absorber tuning, by passive [1], semi-active [2], or active methods, [3], is a relatively straightforward task and has been widely addressed in literature. In many applications, however, the absorber cannot be placed at the target location due to various constraints. As a typical example we refer to machining, where the absorber cannot be placed at the tip of the cutting tool. In such applications, the vibration absorber needs to be deployed at a different position at the structure. This setting will be referred to in what follows as *non-collocated vibration absorption*. Thus, the vibration (and associated energy) need to propagate through a part of the system's structure before being absorbed. Inevitably, tuning of such an absorber is a considerably more difficult task since the dynamics of the involved part of the system need to be included in the design, [4], [5].

Due to the problem complexity, studies related to non-collocated vibration absorption of a harmonic excitation at frequency ω have been limited so far. In [6] a passive absorber is proposed to suppress vibrations at a remote location. In [7], the stiffness is passively adjusted by assigning zeros $\pm\jmath\omega$ to the *receptance*, i.e. to the transfer function between the excitation force and the target position to be damped, whereas state feedback is applied to achieve closed loop stability. In [8] sprung masses are used to impose the points of zero vibration (so called nodes) for general elastic structures during forced harmonic excitation. Maximum allowable amplitudes were studied in the subsequent work [9]. By applying geometric methods, the authors of [10], [11], derived an active control approach for simultaneous vibration attenuation at two separate locations in a system structure one of which is non-collocated. An electrical dynamic absorber is used in [12] to emulate the behavior of a non-collocated mechanical dynamic absorber on a setup with a flexible beam, see also [13] for an application of a modal filter. A method for non-collocated vibration suppression in a light-weight structure has been proposed recently in [14]. An active control with feedback from the non-collocated measurements is applied to shift the antiresonance frequency of a receptance to the excitation frequency ω. A pole-zero assignment to the receptance valid for the single-input and multi-input setting is proposed in [15].

In the above outlined works, the vibration suppression is achieved either by passive parameter adjustment, or by active feedback control of higher complexity. The method presented in this paper combines structural adjustment of the system and low-complexity control feedback at the active vibration absorber, analogous to feedback used in *Delayed Resonator* (DR). The DR concept was proposed in 1990s by Olgac and his co-workers [16] for the standard collocated vibration absorption task. The time-delay feedback is applied to turn the active absorber into a marginally stable system with imaginary axis characteristic roots matching the excitation frequency, such that the DR acts as a perfect resonator and absorbs the vibration entirely. The resonator feedback can be implemented using position [16], velocity [17], or acceleration [18] measurements at the absorber. Modifications of the resonator concept include a torsional absorber [19], and an auto-tuning algorithm to enhance the robustness against uncertainties [20]. A complete dynamics analysis of the DR was performed in [21] for the case of lumped delayed acceleration feedback, leading to a time delay system with neutral spectrum, and in [22] for the case of distributed delayed acceleration feedback, leading to a time delay system with retarded spectrum. The analysis was further extended in [23] to DRs with position and velocity feedback, where the system's spectrum is also retarded. From the stability analysis investigated in [23], it was demonstrated that if not tuned properly, the DR can considerably lower the stability margin or destabilize the overall system even for its collocated deployment. A way to handle this issue consists of the application of a multi-parameter DR feedback as proposed in [24], where the stability constraint is included in the optimal design of a robust DR. Alternatively, an additional control loop can be included to regain and robustify the stability, as proposed in [25], while also increasing robustness with respect to frequency mismatch by placing a double root at the nominal frequency. Other recent research directions include combining position and velocity feedback [26], optimizing the resonator with multiple distributed delays [27], targeting two frequencies [28], the deisgn of fractional-order DRs [29], supplementing the DR with an amplifying mechanism [30], and the dimensional extension of the concept to 2D [31], [32], and 3D [33], [34]. In [35] a delay free, but filtered, proportional-integral acceleration feedback of the absorber was elaborated. In [36], the concept of *linear active resonator* (LAR) was

proposed by Filipovic and Schröder. Conceptually, it mirrors the DR structure with a tuneable gain, which, however, is placed in series with a rational transfer function instead of the delayed term used in DR.

Recently, Olgac and Jenkins demonstrated that the DR is applicable for non-collocated vibration absorption of a system composed of a serial interconnection of flexibly linked masses [4], [5], as shown in Fig. 1. However, compared to the collocated DR design, part of the primary structure needs to be included in tuning the two parameters of the DR feedback. The DR together with this part of the primary form a *resonant substructure*, which needs be tuned as a whole. Thus, the pole couple $\pm\jmath\omega$, which becomes an active zero of the receptance, is to be assigned to the whole resonant substructure. Although such a pole placement is a relatively straightforward task, due to an increase of the structural complexity, the risk of stability loss of the whole system is even higher compared to the collocated case. It was also discussed in [4], [5] that the resonant substructure can only be defined in special system configurations, including the nominally analysed series of the masses. Note that the findings of Olgac and Jenkins confirm the earlier results by Filipovic and Schröder presented in [37], where an analogous problem of remote (non-collocated) vibration suppression at a system composed of a series of flexibly linked masses is solved by the LAR. Next to the theoretical analysis performed over the receptance transfer functions, an experimental validation is performed for the two-mass setup.

In [38], a generally applicable spectral design of non-collocated vibration suppression performed primarily by a DR is presented. The vibration suppression is achieved by direct assignment of the receptance zeros to $\pm\jmath\omega$. In order to increase the stability margin, a stabilizing controller can be included and tuned by spectral optimization. Compared to the method of [4], [5], the method proposed in [38] does not require the existence of a resonating substructure. On the other hand, a part where absorbed energy is accumulated cannot be identified for this general setting as a rule. The proposed method has been validated on an experimental setup with three masses and a resonator actuated by voice-coils. In a subsequent work [39], an output feedback controller is used to assign the active zero couple and to stabilize the system with feedback delay. The synthesis is performed by spectral

optimization and the results are also validated experimentally. In [40] the simultaneous zero assignment and stabilization in the non-collocated setting is achieved by a DR with multiple delay static feedback. A DR with delayed dynamic-feedback controller is proposed in [41] to target multi-frequency non-collocated vibration absorption.

Despite the above discussed development of generally applicable methods [38], [39], [40], [41], the serial configuration addressed in [4], [5] and [37] deserves further attention and deeper analysis as it is the configuration often met in practice. In [4], [5], it was shown that for given parameters of the system and the DR, only frequencies that correspond to stability regions in the parameter set can be successfully suppressed. Another important observation and a problem opened in [4] and [5] concern fatigue loading across the structure. It was demonstrated by simulations, that, as a consequence of suppressing vibrations at the non-collocated target mass, the amplitudes of the steady-state oscillations across the structure either increase or decrease compared to the passive case. Therefore, it imposes either higher or lesser fatigue loading.

The main objective of this paper is to address the two potentially risky features of non-collocated vibration absorption identified by Olgac and Jenkins in the design methodology, [4], [5], i.e., increased fatigue loading and impact on stability. Additionally, we aim at minimization of energy needs by the DR in the non-collocated vibration absorption task. Through detailed analysis of system model in phasor form, in Section 2, we show that for given parameters of the primary, the fatigue loading across the structure can be changed neither by choosing an alternative control method nor by redesigning the absorber parameters. It can only be changed by modifying the parameters of the structure. Such parameter adjustment can also be beneficial towards either gaining or strengthening stability of the structure with non-collocated DR. Next, in terms of decomposed phasor model characteristics, we provide the DR feedback synthesis and assessment of energy needed for the non-collocated vibration absorption. Utilizing these characteristics, an integrated design procedure is proposed in Section 3 for the simultaneous optimization of the system's structural properties and the DR's feedback loop. For a given excitation frequency ω, the objectives are set as: i) suppress fully vibration at the target non-collocated location with a sufficient stability

margin, ii) minimize fatigue loading at the most risky place at the system structure, and iii) minimize the power needed for vibration suppression by the active feedback. The objective i) is turned to constraints, whereas the objectives ii) and iii) are balanced within the objective function. This leads to a constrained nonlinear optimization problem to be solved. Two case studies are included to demonstrate and validate the proposed results. In Section 4, the mechanisms by which the optimized parameters influence the optimization objectives is demonstrated and experimentally validated on a mechatronic set-up with three masses. Consequently, for a more complex system structure with five masses, a thorough numerical case study is performed in Section 5. It is shown that the constrained nonlinear optimization problem can in principle be solved by recently proposed GRANSO tool [42], utilizing functionalities of the TDS-CONTROL toolbox [43]. Conclusions and future research directions are stated in Section 6.

2. System structural analysis and delayed resonator design

Assume a linear chain of d flexibly linked masses m_i as shown in Fig. 1 a). Each mass m_i with position x_i is connected to its predecessor via a spring k_i and a dumper c_i. The first and the last masses (m_1 and m_d) are connected to a base. Assume the ω-harmonic disturbance force

$$f_d(t) = \bar{f}_d \cos \omega t \tag{1}$$

with amplitude $\bar{f}_d$ acts on mass m_d. The objective is to fully suppress vibration of the mass m_s. It is to be done by an active *vibration absorber* with mass m_a, position x_a, damping c_a, and stiffness k_a, and an active control force $u(t)$. The absorber is deployed at the mass m_p. In the analysis which follows, we assume $p < s \leq d$, implying solution of *non-collocated vibration absorption* problem. The case, where $p = s$ degrades to the standard problem of *collocated vibration absorption*, thoroughly analyzed, e.g., in [23]. Note also that for $p < s = d$, i.e., the periodic force is acting directly on mass m_s, which substantially simplifies the problem to be solved, as demonstrated below.

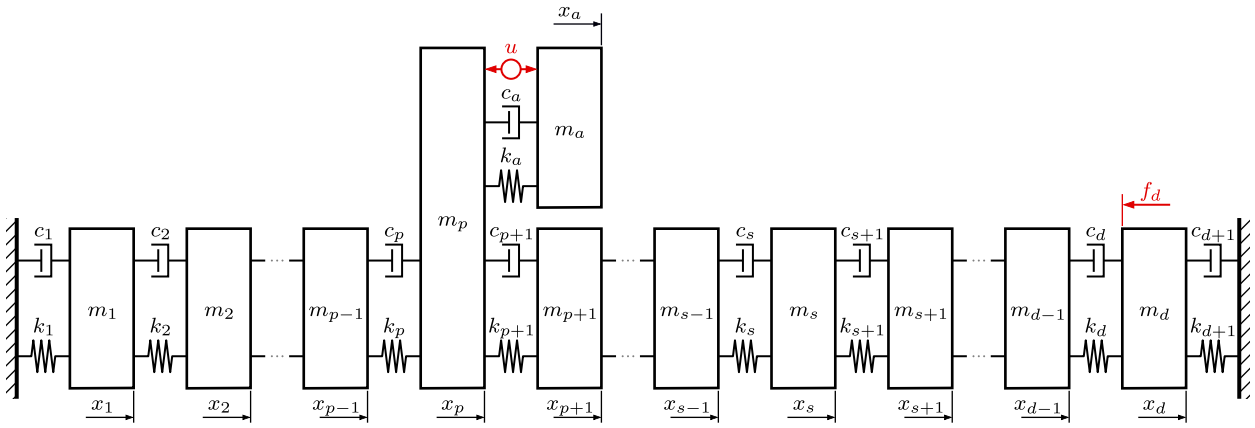

(a) The overall system of flexibly linked masses being excited by an ω-harmonic force f_d, with an active absorber m_a mounted at mass m_a, and the objective to ideally suppress vibration at the mass m_s

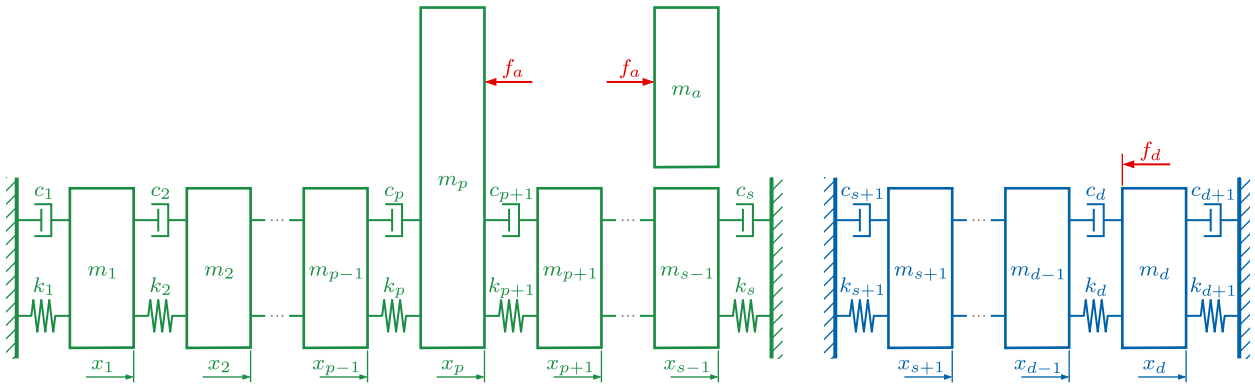

(b) Separation of the system when the vibration at the mass m_s is ideally suppressed (i.e., it can be considered as a motion-less barrier) into i) a *resonating subsystem (green) excited by f_a, ii)* vibrating subsystem (blue) excited by f_d, and iii) *absorber being excited by f_a.*

Figure 1: System configuration and its structural decomposition.

For analytical purposes, let us introduce a *total force in the absorber's link* as

$$f_a(t) = u(t) + k_a(x_p(t) - x_a(t)) + c_a(\dot{x}_p(t) - \dot{x}_a(t)), \tag{2}$$

which allows us to free the absorber mass m_a from the mass m_p, as shown in Fig. 1 b). The system of linked masses $m_i,\ i = 1, \ldots, d$ can then be described by a set of d second-order linear equations

$$\mathbf{M}\ddot{\mathbf{x}}(t) + \mathbf{C}\dot{\mathbf{x}}(t) + \mathbf{K}\mathbf{x}(t) = \mathbf{B}_d f_d(t) + \mathbf{B}_a f_a(t), \tag{3}$$

where $\mathbf{x}(t)$ is vector of displacements $x_i,\ i = 1, \ldots, d$, *mass matrix* $\mathbf{M}$ is of a diagonal form

$$\mathbf{M} = \mathrm{diag}\left(m_1, m_2, \ldots, m_p, \ldots, m_s, \ldots, m_{d-1}, m_d\right). \tag{4}$$

Defining $\mathbf{k} = [k_2, \ldots, k_p, \ldots, k_s, \ldots, k_{d-1}, k_d]$, and denoting zero column vector of length n as $\mathbf{o}_n$, the *stiffness matrix* has the tridiagonal structure

$$\mathbf{K} = \mathrm{diag}([k_1\ \mathbf{k}]) + \mathrm{diag}([\mathbf{k}\ k_{d+1}]) - \begin{bmatrix} \mathbf{o}_{d-1} & \mathrm{diag}(\mathbf{k}) \\ 0 & \mathbf{o}_{d-1}^{\mathrm{T}} \end{bmatrix} - \begin{bmatrix} \mathbf{o}_{d-1}^{\mathrm{T}} & 0 \\ \mathrm{diag}(\mathbf{k}) & \mathbf{o}_{d-1} \end{bmatrix}, \tag{5}$$

and *damping matrix* $\mathbf{C}$ is of the same structure as $\mathbf{K}$, provided that each spring stiffness k_i is replaced by the corresponding damping c_i. The system input matrices are given by

$$\mathbf{B}_d = \begin{bmatrix} \mathbf{o}_{d-1}^{\mathrm{T}} & 1 \end{bmatrix}^{\mathrm{T}}, \tag{6}$$

and

$$\mathbf{B}_a = \begin{bmatrix} \mathbf{o}_{p-1}^{\mathrm{T}} & 1 & \mathbf{o}_{d-p}^{\mathrm{T}} \end{bmatrix}^{\mathrm{T}}. \tag{7}$$

In order to study the steady-state harmonic motion of the masses at the frequency ω, let us turn the harmonic force (1) to

$$f_d(t) = \Re\{\vec{f_d} e^{\jmath\omega t}\}, \tag{8}$$

with $\vec{f_d}$ being a phasor. The overall system (3) can then be transformed to

$$\mathbf{A}(\omega)\vec{\mathbf{x}} = \mathbf{B}_d\vec{f_d} + \mathbf{B}_a\vec{f_a}, \tag{9}$$

where the *dynamic stiffness characteristic matrix* is given by

$$\mathbf{A}(\omega) = -\mathbf{M}\omega^2 + \mathbf{C}\jmath\omega + \mathbf{K}. \tag{10}$$

From (9) the phasor representing the displacement of mass m_i can be expressed as

$$\vec{x_i} = \mathbf{e}_i^{\mathrm{T}}\mathbf{A}^{-1}(\omega)\left(\mathbf{B}_d\vec{f_d} + \mathbf{B}_a\vec{f_a}\right), \tag{11}$$

where $\mathbf{e}_i = \begin{bmatrix} \mathbf{o}_{i-1}^{\mathrm{T}} & 1 & \mathbf{o}_{d-i}^{\mathrm{T}} \end{bmatrix}^{\mathrm{T}}$ encodes the position of mass m_i with respect to the whole chain of masses.

Considering the objective of stopping mass m_s, with a reference to Fig. 1, the system can be split into three subsystems: i) the *resonating subsystem* given by the masses $m_j,\ j = 1, 2, \ldots, s-1$; ii) the *target mass* m_s to be stopped; and iii) the *vibrating subsystem* given by masses $m_k,\ k = s+1, s+2, \ldots, d$. Respecting this subsystem division, the vector of displacements phasor is formed as

$$\vec{\mathbf{x}} = \begin{bmatrix} \vec{\mathbf{x}}_R^{\mathrm{T}} & \vec{x}_s & \vec{\mathbf{x}}_V^{\mathrm{T}} \end{bmatrix}^{\mathrm{T}}, \tag{12}$$

where $\vec{\mathbf{x}}_R = \begin{bmatrix} \vec{x}_1 & \ldots & \vec{x}_{s-1} \end{bmatrix}^{\mathrm{T}}$ and $\vec{\mathbf{x}}_V = \begin{bmatrix} \vec{x}_{s+1} & \ldots & \vec{x}_d \end{bmatrix}^{\mathrm{T}}$ are vectors of displacements of resonating and vibrating subsystems, respectively. Analogously, we can express the dynamic stiffness matrix as

$$\mathbf{A}(\omega) = \begin{bmatrix} \mathbf{A}_R(\omega) & \mathbf{a}_R(\omega) & \mathbf{0} \\ \mathbf{a}_R^{\mathrm{T}}(\omega) & a_{s,s}(\omega) & \mathbf{a}_V^{\mathrm{T}}(\omega) \\ \mathbf{0} & \mathbf{a}_V(\omega) & \mathbf{A}_V(\omega) \end{bmatrix}, \tag{13}$$

where $\mathbf{a}_R^{\mathrm{T}} = \begin{bmatrix} \mathbf{o}_{s-1}^{\mathrm{T}} & -\jmath\omega c_s - k_s \end{bmatrix}$ and $\mathbf{a}_V^{\mathrm{T}} = \begin{bmatrix} -\jmath\omega c_{s+1} - k_{s+1} & \mathbf{o}_{d-s}^{\mathrm{T}} \end{bmatrix}$ represent links from vibrating and resonating subsystem to target mass m_s, respectively. Input matrices are defined as

$$\mathbf{B}_d = \begin{bmatrix} \mathbf{o}_{s-1}^{\mathrm{T}} & 0 & \mathbf{D}_d^{\mathrm{T}} \end{bmatrix}^{\mathrm{T}}, \tag{14}$$

$$\mathbf{B}_a = \begin{bmatrix} \mathbf{D}_a^{\mathrm{T}} & 0 & \mathbf{o}_{d-s}^{\mathrm{T}} \end{bmatrix}^{\mathrm{T}}, \tag{15}$$

where $\mathbf{D}_d = \begin{bmatrix} \mathbf{o}_{d-s-1}^{\mathrm{T}} & 1 \end{bmatrix}^{\mathrm{T}}$ and $\mathbf{D}_a = \begin{bmatrix} \mathbf{o}_{p-1}^{\mathrm{T}} & 1 & \mathbf{o}_{s-p}^{\mathrm{T}} \end{bmatrix}^{\mathrm{T}}$.

2.1. Force and motion balance at the target stage

Assume the *target stage* with

$$\vec{x}_s = 0 \tag{16}$$

is reached thanks to the active absorber action fully compensating the effect of excitation force (8). Then, as indicated in Fig. 1b, the mass m_s can be considered as a motion-less barrier and the system can be split into *vibrating subsystem*

$$\mathbf{A}_V(\omega)\vec{\mathbf{x}}_V = \mathbf{D}_d\vec{f}_d, \tag{17}$$

and *resonating subsystem*

$$\mathbf{A}_R(\omega)\vec{\mathbf{x}}_R = \mathbf{D}_a\vec{f}_a. \tag{18}$$

The relation between the required force $\vec{f}_a$ and disturbance force $\vec{f}_d$ is clarified in the following proposition.

Proposition 1. *Assume the system* (3) *turned into the phasor form* (9)*, with the output* (12)*, and matrices* (13)*,* (14) *and* (15)*, is excited by a harmonic force f_d with frequency ω given in* (8)*. Furthermore, assume $p < s \leq d$, $a_{s,s} \neq 0$ and invertibility of submatrices $\mathbf{A}_R(\omega)$ and $\mathbf{A}_V(\omega)$. Then, as soon as the motion of the* target mass *m_s is perfectly stopped (i.e. $\vec{x}_s = 0$) the phasor of the total force in the absorber's link is given by*

$$\vec{f}_a = -\left(\mathbf{a}_V^{\mathrm{T}}(\omega)\mathbf{A}_V^{-1}(\omega)\mathbf{D}_d\right)\left(\mathbf{a}_R^{\mathrm{T}}(\omega)\mathbf{A}_R^{-1}(\omega)\mathbf{D}_a\right)^{-1}\vec{f}_d, \tag{19}$$

for $p < s < d$ and by

$$\vec{f}_a = \left(\mathbf{a}_R^{\mathrm{T}}(\omega)\mathbf{A}_R^{-1}(\omega)\mathbf{D}_a\right)^{-1}\vec{f}_d, \tag{20}$$

for $p < s = d$.

Proof. For $p < s < d$, we rewrite the system (9) into

$$\mathbf{A}_R(\omega)\vec{\mathbf{x}}_R + \mathbf{a}_R(\omega)\vec{x}_s = \mathbf{D}_a\vec{f}_a, \tag{21}$$

$$\mathbf{a}_R^{\mathrm{T}}(\omega)\vec{\mathbf{x}}_R + a_{s,s}(\omega)\vec{x}_s + \mathbf{a}_V^{\mathrm{T}}(\omega)\vec{\mathbf{x}}_V = 0, \tag{22}$$

$$\mathbf{a}_R(\omega)\vec{x}_s + \mathbf{A}_V(\omega)\vec{\mathbf{x}}_V = \mathbf{D}_d\vec{f}_d. \tag{23}$$

Substituting $\vec{x}_s = 0$ to (21), (22) and (23), and solving (21) for $\vec{\mathbf{x}}_R$, and (23) for $\vec{\mathbf{x}}_V$, respectively, yields

$$\vec{\mathbf{x}}_R = \mathbf{A}_R^{-1}(\omega)\mathbf{D}_a\vec{f}_a, \tag{24}$$

and

$$\vec{\mathbf{x}}_V = \mathbf{A}_V^{-1}(\omega)\mathbf{D}_d\vec{f}_d. \tag{25}$$

Substituting (24) and (25) into (22) and expressing $\vec{f_a}$ gives (19).

For the case $p < s = d$, system of equations degenerates to

$$\mathbf{A}_R(\omega)\vec{\mathbf{x}}_R + \mathbf{a}_R(\omega)\vec{x}_s = \mathbf{D}_a\vec{f_a}, \tag{26}$$

$$a_{s,s}(\omega)\vec{x}_s + \mathbf{a}_R^{\mathrm{T}}(\omega)\vec{\mathbf{x}}_R = \vec{f_d}. \tag{27}$$

Analogously as in the above case, substituting $\vec{x}_s = 0$ to (26) and (27) and eliminating $\vec{\mathbf{x}}_R$ from the equation set, yields (20). □

2.2. Fatigue loading expressed in terms of elastic potential energy at the links

In general, stopping the mass m_s leads to a redistribution of the oscillation amplitudes among the remaining masses. In some cases, it can go above safe limit and even cause damage due to accumulated fatigue. In order to assess this risk, let us express the elastic potential energy in i^{th}-link as

$$W_i(t) = \frac{1}{2}k_i\left(x_i(t) - x_{i-1}(t)\right)^2, \tag{28}$$

which can be considered as a measure to evaluate the risk of fatigue.

Let $\Delta x_{i,i-1}(t) = x_i(t) - x_{i-1}(t)$ and let $\Delta\vec{x}_{i,i-1}$ denote the corresponding phasor. Then we can express $\Delta x_{i,i-1}(t) = |\Delta\vec{x}_{i,i-1}|\cos(\omega t + \varphi)$ with $\varphi = \angle\left(\Delta\vec{x}_{i,i-1}\right)$ and

$$W_i(t) = \frac{1}{2}k_i\left|\Delta\vec{x}_{i,i-1}\right|^2\cos^2(\omega t + \varphi) = \frac{1}{4}k_i\left|\Delta\vec{x}_{i,i-1}\right|^2\left(1 + \cos(2\omega t + 2\varphi)\right).$$

The latter expression can be written in the form

$$W_i(t) = \bar{W}_{i,\mathrm{mean}} + \Re\left\{\vec{W}_i e^{\jmath 2\omega t}\right\}, \tag{29}$$

where the first term denotes the average elastic energy,

$$\bar{W}_{i,\mathrm{mean}} = \frac{1}{4}k_i\left|\Delta\vec{x}_{i,i-1}\right|^2, \tag{30}$$

and

$$\vec{W}_i = \frac{1}{4}k_i\left(\Delta\vec{x}_{i,i-1}\right)^2 \tag{31}$$

can be interpreted as a phasor rotating with doubled frequency. The maximal elastic energy satisfies

$$W_{i,\max} = \bar{W}_{i,\text{mean}} + |\vec{W}_i| \tag{32}$$

$$= \frac{1}{2} k_i \left|\Delta \vec{x}_{i,i-1}\right|^2 \tag{33}$$

$$= \frac{1}{2} k_i \left| \left(\mathbf{e}_i^{\mathrm{T}} - \mathbf{e}_{i-1}^{\mathrm{T}}\right) \mathbf{A}^{-1}(\omega) \left(\mathbf{B}_d \vec{f}_d + \mathbf{B}_a \vec{f}_a\right) \right|^2 . \tag{34}$$

Note that the elastic potential energies in links between masses and base are solved by explicitly setting $\mathbf{e}_0 = \mathbf{e}_{d+1} = \mathbf{o}_d$.

When the final stage is reached, maximal values of the elastic potential energies can be simplified as given in the following proposition.

Proposition 2. *When the final stage is reached, the maximal elastic potential energy in the ith-link of the resonating subsystem is given by*

$$W_{i,\max} = \frac{1}{2} k_i \left| \left(\mathbf{e}_{r,i}^{\mathrm{T}} - \mathbf{e}_{r,i-1}^{\mathrm{T}}\right) \mathbf{A}_R^{-1}(\omega) \mathbf{D}_a \vec{f}_a \right|^2, \quad 1 \le i \le s, \tag{35}$$

while for the jth-link of vibrating subsystem, it is given by

$$W_{j,\max} = \frac{1}{2} k_j \left| \left(\mathbf{e}_{v,j}^{\mathrm{T}} - \mathbf{e}_{v,j-1}^{\mathrm{T}}\right) \mathbf{A}_V^{-1}(\omega) \mathbf{D}_d \vec{f}_d \right|^2, \quad s+1 \le j \le d+1, \tag{36}$$

where $\mathbf{e}_{r,i} = \begin{bmatrix} \mathbf{o}_{i-1}^{\mathrm{T}} & 1 & \mathbf{o}_{s-i-1}^{\mathrm{T}} \end{bmatrix}^{\mathrm{T}}$ and $\mathbf{e}_{v,j} = \begin{bmatrix} \mathbf{o}_{s-j-1}^{\mathrm{T}} & 1 & \mathbf{o}_{d-j}^{\mathrm{T}} \end{bmatrix}^{\mathrm{T}}$ encode the position of the mass m_i in the resonating subsystem and the position of the mass m_j in vibrating subsystem, respectively. The links at the base are handled via setting $\mathbf{e}_{r,0} = \mathbf{e}_{r,s} = \mathbf{o}_{s-1}$ for the resonating subsystem, and $\mathbf{e}_{v,s} = \mathbf{e}_{v,d+1} = \mathbf{o}_{d-s-1}$ for vibrating subsystem.

Proof. For resonating subsystem, i.e. $0 < i \le s$, we rewrite (24) to

$$\vec{x}_i = \mathbf{e}_{r,i}^{\mathrm{T}} \mathbf{A}_R^{-1}(\omega) \mathbf{D}_a \vec{f}_a, \tag{37}$$

which can be directly substituted to (33) yielding (35).

Analogously for vibrating subsystem, i.e. $s < j \le d+1$, we can rewrite (25) to

$$\vec{x}_j = \mathbf{e}_{v,j}^{\mathrm{T}} \mathbf{A}_V^{-1}(\omega) \mathbf{D}_d \vec{f}_d, \tag{38}$$

and substitute it to (33) to obtain (36). □

Combining results from Propositions 1 and 2 allows us to form the following Theorem.

Theorem 1. *The maximal elastic potential energies at the final stage defined in* (35) *and* (36) *only depend on the disturbance force (specifically on frequency* ω *and amplitude* $\bar{f}_d$*) and mass, damping, and stiffness parameters within the resonating and vibrating subsystems.*

Corollary 1. *The elastic potential energies cannot be redistributed by the control authority of the resonator. The only way for its redistribution is via a structural optimization of both the vibrating and the resonating subsystems.*

Remark 1. *Expression* (19) *and* (20) *can be written in the form*

$$\vec{f}_a = -\mathbf{G}_1(\jmath\omega)^{-1}\mathbf{G}_2(\jmath\omega)\vec{f}_d \tag{39}$$

where $\mathbf{G}_1$ *and* $\mathbf{G}_2$ *are the transfer functions from* $\vec{f}_a$ *and* $\vec{f}_d$ *to the position of the target* $\vec{x}_s$*. The expression* (39) *is also applicable to more complex topologies than linear chains, including topologies where a separation into resonating and vibrating subsystems is not possible. Consequently, Theorem 1 remains valid in such cases.*

2.3. Delayed resonator analysis and design

Let us note that both the above propositions hold true regardless of how the force f_a is generated. In what follows we consider the traditional DR with position feedback. Though, the modification to DR with velocity or acceleration feedback is straightforward. With a reference to Fig. 1a, the dynamics of the absorber is governed by

$$m_a\ddot{x}_a(t) = f_a(t), \tag{40}$$

which in the phasor form reads as

$$-m_a\omega^2\vec{x}_a = \vec{f}_a, \tag{41}$$

and implies

$$\vec{x}_a = -\frac{1}{m_a\omega^2}\vec{f}_a. \tag{42}$$

Dynamics of DR can be obtained by substituting (2) into (40)

$$m_a\ddot{x}_a(t) + c_a\dot{x}_a(t) + k_a x_a(t) = c_a\dot{x}_p(t) + k_a x_p(t) + u(t), \tag{43}$$

where the delayed position feedback is considered in the form

$$u(t) = g x_a(t-\tau), \tag{44}$$

with tuneable gain g and time delay $\tau \geq 0$.

Proposition 3. *The force f_a given by (19) needed for complete vibration suppression of the mass m_s excited by the force f_d given by (1) and acting at the mass m_d can be generated by the DR (43)–(44) with a parameter pair g, τ from the sets*

$$g^+ = |Q(\omega)|, \quad \tau^+ = \frac{1}{\omega}(-\arg Q(\omega) + 2k\pi), k \in Z, \tag{45}$$

$$g^- = -|Q(\omega)|, \quad \tau^- = \frac{1}{\omega}(\pi - \arg Q(\omega) + 2k\pi), k \in Z, \tag{46}$$

with

$$Q(\omega) = -m_a\omega^2\left[1 - (\jmath\omega c_a + k_a)\left(\mathbf{e}_{r,p}^{\mathrm{T}}\mathbf{A}_R^{-1}(\omega)\mathbf{D}_a + \frac{1}{m_a\omega^2}\right)\right], \tag{47}$$

provided that the overall setup is stable and feedback with the selected pair g, τ is realizable, i.e. $\tau \geq 0$.

Proof. Both (43) and (44) can be expressed in the phasor form as

$$-m_a\omega^2\vec{x}_a = (\jmath\omega c_a + k_a)(\vec{x}_p - \vec{x}_a) + \vec{u}, \tag{48}$$

$$\vec{u} = g e^{-\jmath\omega\tau}\vec{x}_a. \tag{49}$$

From (24) we can express the phasor of position of mass m_p as

$$\vec{x}_p = \mathbf{e}_{r,p}^{\mathrm{T}}\mathbf{A}_R^{-1}(\omega)\mathbf{D}_a\vec{f}_a, \tag{50}$$

where $\mathbf{e}_{r,p}^{\mathrm{T}} = \begin{bmatrix}\mathbf{o}_{p-1}^{\mathrm{T}} & 1 & \mathbf{o}_{s-p}^{\mathrm{T}}\end{bmatrix}$. Substituting (41), (42) and (50) into (48) and expressing $\vec{u}$ as a function of $\vec{f}_a$ gives

$$\vec{u} = \left[1 - (\jmath\omega c_a + k_a)\left(\mathbf{e}_{r,p}^{\mathrm{T}}\mathbf{A}_R^{-1}(\omega)\mathbf{D}_a + \frac{1}{m_a\omega^2}\right)\right]\vec{f}_a. \tag{51}$$

Substituting (42) to (49) yields

$$\vec{u} = -\frac{g}{m_a\omega^2} e^{-\jmath\omega\tau} \vec{f}_a. \tag{52}$$

Comparing (51) and (52) with both sides multiplied by $-m_a\omega^2$ then gives

$$g e^{-\jmath\omega\tau} = Q(\omega), \tag{53}$$

where $Q(\omega)$ is of a form (47) given in proposition. Comparing the magnitude and the argument of both sides of (53) yields parameters of the DR. □

In [23], it was derived for the collocated deployment of the DR that the best stability posture and robustness against nominal and true frequency mismatch is achieved for the first delay branch. Analogous result can be expected for the non-collocated case under consideration. Therefore, as a rule of thumb, the pair with the lowest positive delay τ is selected.

Similarly to the preceding section, the potential risk of fatigue in the DR's link is quantified by the maximal elastic potential energy between the system mass m_p and the absorber mass m_a at the stage of equilibrium oscillations. Using (28) and substituting the positions x_a and x_p yields

$$W_a(t) = \bar{W}_{a,\text{mean}} + \Re\left\{\vec{W}_a e^{\jmath 2\omega t}\right\}, \tag{54}$$

where, assuming $\Delta\vec{x}_{a,p} = \vec{x}_a - \vec{x}_p$, time independent average is defined as

$$\bar{W}_{a,\text{mean}} = \frac{1}{4} k_a \left|\Delta\vec{x}_{a,p}\right|^2, \tag{55}$$

and phasor as

$$\vec{W}_a = \frac{1}{4} k_a \left(\Delta\vec{x}_{a,p}\right)^2, \tag{56}$$

with maximal value

$$W_{a,\max} = \bar{W}_{a,\text{mean}} + |\vec{W}_a|, \tag{57}$$

$$= \frac{1}{2} k_a \left| \left(-\frac{1}{m_a\omega^2} - \mathbf{e}_{r,p}^{\mathrm{T}} \mathbf{A}_R^{-1}(\omega) \mathbf{D}_a \right) \vec{f}_a \right|^2. \tag{58}$$

2.3.1. Actuation power assessment needed for full vibration suppression

The actuation power at the DR's control feedback is given by

$$p(t) = u(t)(\dot{x}_p(t) - \dot{x}_a(t)), \tag{59}$$

which can not be represented by phasor, however can be rewritten to

$$p(t) = \bar{p}_{\text{mean}} + \Re\{\vec{p}e^{\jmath 2\omega t}\}, \tag{60}$$

where the first part of right hand side

$$\bar{p}_{\text{mean}} = \frac{1}{2}\Re\{\jmath\omega(\vec{u})^* (\vec{x}_p - \vec{x}_a)\} \tag{61}$$

is independent on time and determines the average value of the power, and

$$\vec{p} = \frac{1}{2}\jmath\omega\vec{u}\,(\vec{x}_p - \vec{x}_a) \tag{62}$$

oscillates with a frequency 2ω with an amplitude

$$\bar{p} = \frac{1}{2}\omega\left|\vec{u}\,(\vec{x}_p - \vec{x}_a)\right|. \tag{63}$$

Thus, the maximum power needed in the steady oscillation stage is given by

$$P_{\max} = \max\left\{|\bar{p} + \bar{p}_{\text{mean}}|, |\bar{p} - \bar{p}_{\text{mean}}|\right\}. \tag{64}$$

2.4. Stability analysis

The necessary condition for achieving the entire vibration suppression at the mass m_s is the stability of the overall system consisting of the series of linked masses and the DR. The stability of the whole system can be checked by determining the rightmost characteristic roots of the system, e.g. by MATLAB package *TDS-CONTROL* [43], [44]. For that purpose, the system model is to be turned to the set of Delay Differential Algebraic Equations (DDAE). First, redefine the state vector of (3) as

$$\overline{\mathbf{x}}(t) = \left[\mathbf{x}(t)^{\mathrm{T}} \quad \dot{\mathbf{x}}(t)^{\mathrm{T}}\right]^{\mathrm{T}}, \tag{65}$$

and rewrite (3) to

$$\begin{bmatrix} \mathbf{I} & \mathbf{0} \\ \mathbf{0} & \mathbf{M} \end{bmatrix} \dot{\overline{\mathbf{x}}}(t) = \begin{bmatrix} \mathbf{0} & \mathbf{I} \\ -\mathbf{K} & -\mathbf{C} \end{bmatrix} \overline{\mathbf{x}}(t) + \begin{bmatrix} \mathbf{o}_d \\ \mathbf{B}_a \end{bmatrix} f_a(t) + \begin{bmatrix} \mathbf{o}_d \\ \mathbf{B}_d \end{bmatrix} f_d(t). \tag{66}$$

Analogously, define the state vector of the absorber as

$$\overline{\mathbf{x}}_a(t) = \begin{bmatrix} x_a(t) & \dot{x}_a(t) \end{bmatrix}^{\mathrm{T}}, \tag{67}$$

and rewrite (40) to

$$\begin{bmatrix} 1 & 0 \\ 0 & m_a \end{bmatrix} \dot{\overline{\mathbf{x}}}_a(t) = \begin{bmatrix} 0 & 1 \\ 0 & 0 \end{bmatrix} \overline{\mathbf{x}}_a(t) + \begin{bmatrix} 0 \\ 1 \end{bmatrix} f_a(t). \tag{68}$$

Further on, equation (2) can be turned to the form

$$0 = \begin{bmatrix} k_a \mathbf{e}_p^{\mathrm{T}} & c_a \mathbf{e}_p^{\mathrm{T}} \end{bmatrix} \overline{\mathbf{x}}(t) + \begin{bmatrix} -k_a & -c_a \end{bmatrix} \overline{\mathbf{x}}_a(t) + u(t) - f_a(t), \tag{69}$$

and the control law (44) can be turned to

$$0 = g \begin{bmatrix} 1 & 0 \end{bmatrix} \overline{\mathbf{x}}_a(t - \tau) - u(t). \tag{70}$$

Defining the extended state vector

$$\tilde{\mathbf{x}}(t) = \begin{bmatrix} \mathbf{x}^{\mathrm{T}}(t) & \dot{\mathbf{x}}^{\mathrm{T}}(t) & x_a(t) & \dot{x}_a(t) & f_a(t) & u(t) \end{bmatrix}^{\mathrm{T}}, \tag{71}$$

the DDAE model for (66), (68), (69) and (70) is as follows,

$$\mathcal{E}\dot{\tilde{\mathbf{x}}}(t) = \mathcal{A}_0 \tilde{\mathbf{x}}(t) + \mathcal{A}_1 \tilde{\mathbf{x}}(t - \tau) + \mathcal{B} f_d(t), \tag{72}$$

where

$$\mathcal{E} = \operatorname{diag}(\mathbf{I}, \mathbf{M}, 1, m_a, 0, 0), \ \mathcal{B} = \begin{bmatrix} \mathbf{o}_d^{\mathrm{T}} & \mathbf{B}_d^{\mathrm{T}} & 0 & 0 & 0 & 0 \end{bmatrix}^{\mathrm{T}},$$

$$\mathcal{A}_0 = \begin{bmatrix} \mathbf{0} & \mathbf{I} & \mathbf{o}_d & \mathbf{o}_d & \mathbf{o}_d & \mathbf{o}_d \\ -\mathbf{K} & -\mathbf{C} & \mathbf{o}_d & \mathbf{o}_d & \mathbf{B}_a & \mathbf{o}_d \\ \mathbf{o}_d^{\mathrm{T}} & \mathbf{o}_d^{\mathrm{T}} & 0 & 1 & 0 & 0 \\ \mathbf{o}_d^{\mathrm{T}} & \mathbf{o}_d^{\mathrm{T}} & 0 & 0 & -1 & 0 \\ k_a \mathbf{e}_p^{\mathrm{T}} & c_a \mathbf{e}_p^{\mathrm{T}} & -k_a & -c_a & -1 & 1 \\ \mathbf{o}_d^{\mathrm{T}} & \mathbf{o}_d^{\mathrm{T}} & 0 & 0 & 0 & -1 \end{bmatrix}, \ \mathcal{A}_1 = \begin{bmatrix} \mathbf{0} & \mathbf{0} & \mathbf{o}_d & \mathbf{o}_d & \mathbf{o}_d & \mathbf{o}_d \\ \mathbf{0} & \mathbf{0} & \mathbf{o}_d & \mathbf{o}_d & \mathbf{o}_d & \mathbf{o}_d \\ \mathbf{o}_d^{\mathrm{T}} & \mathbf{o}_d^{\mathrm{T}} & 0 & 0 & 0 & 0 \\ \mathbf{o}_d^{\mathrm{T}} & \mathbf{o}_d^{\mathrm{T}} & 0 & 0 & 0 & 0 \\ \mathbf{o}_d^{\mathrm{T}} & \mathbf{o}_d^{\mathrm{T}} & 0 & 0 & 0 & 0 \\ \mathbf{o}_d^{\mathrm{T}} & \mathbf{o}_d^{\mathrm{T}} & g & 0 & 0 & 0 \end{bmatrix}.$$

The dynamic behavior of the controlled system (72) is governed by

$$P(\lambda) = \det\left(\mathcal{E}\lambda - \mathcal{A}_0 - \mathcal{A}_1 e^{-\lambda\tau}\right), \tag{73}$$

which in general has infinitely many roots. The stability is implied by the location of all the roots in the left hand side of complex plane. Such a condition can be defined in a compact way via introducing the *spectral abscissa*

$$\alpha = \max_{\lambda\in\mathbb{C}}\{\Re(\lambda) : \ P(\lambda) = 0\}, \tag{74}$$

and requiring $\alpha < 0$.

3. Simultaneous structural optimization and control design

As it results from the above analysis, with a reference to Fig. 1, once the system is being excited by a harmonic force (1) acting on the mass m_d and the mass m_s is to be stopped, there exists a unique control force f_a acting at the mass m_p given in Proposition 1. Thus, as stated in Theorem 1, the motion of masses in both the resonating and vibrating subsystems cannot be influenced by the control authority and they are fully determined by the structural parameters of the setup itself. Consequently, the only way of modifying the potential energy in the links is via the adjustment of parameters $m_i,\ i = 1,\dots,d,\ i \neq s$, and $c_i,\ k_i,\ i = 1,\dots,d+1$.

Besides, considering the two-parameter control rule (44), the parameters of which are by Proposition 3, no degrees of freedom in the DR feedback is left for tuning the closed-loop dynamics. Unlike in [24], [38], [39], [45], where either the set of free parameters in the DR feedback was enlarged or a supplementary stabilizing controller was deployed, we stick to the simple structure DR position feedback (44), which is easy to implement and tune in practice. Thus, the only way to ensure the stability of the considered setting is to include the stability condition in the structural parameter optimization. Also note that the stability constraint would be analogous if we considered DR velocity feedback instead of the DR position feedback. In both cases, the DDAE model would be of retarded type. Considering the acceleration feedback, however, would lead to neutral DDAE. Additionally to standard

stability check of the DDE, the strong stability check of the associated difference equation would be needed.

An additional quantity to follow is the power needed for beating the vibration at the non-collocated mass m_s. As it results from (59), it is determined by a product of velocity difference of masses m_p and m_a and the actuation force of the DR given by (44). Hence, it can be influenced by the parameters of the whole resonating substructure, consisting of the resonating subsystem with masses $m_i,\ i = 1, \ldots, s-1$ and the DR with mass m_a. Additional constraints may arise from the limits on the construction parameters, and safety and durability of the DR which may be more relaxed compared to those characteristics of the system.

To sum up the discussion above, the following objectives and constraints are to be followed in the structural parameter optimization:

1. *Full vibration suppression at the non-collocated mass m_s.* This task is directly fulfilled by the equality constraints defined in Proposition 3 and taking the pair of parameters g, τ with the smallest positive delay τ.

2. *Minimizing the risk of fatigue across the system.* The fatigue is quantified via a potential energy in the system links derived in Proposition 2. The objective is to minimize this quantity at the most risky link, which leads to the solution of the min-max problem:

$$\min\{\max\{W_{i,\max} :\ 1 \leq i \leq d\}\}. \tag{75}$$

3. *Minimizing the maximum of the power needed for the vibration suppression.* This task directly leads to

$$\min\{P_{\max}\}, \tag{76}$$

where $P_{\max}$ is given by (64).

4. *Stability of the overall system.* This can be achieved by considering the constraint

$$\alpha \leq \xi_\alpha \tag{77}$$

where the spectral abscissa α of the DDAE system (72) is given by (74), and $\xi_\alpha < 0$, is a selected distance from the stability boundary, imposing a desired stability margin.

5. *Physical parameter constraints.* Limits on the selected parameters to be optimized (mass, damping and stiffness of the links).

6. *A DR safety and durability constraint.* Assessing the fatigue in the absorber's link in terms of potential energy (58), it leads to the condition

$$W_{a,\max} \leq \xi_a \tag{78}$$

where ξ_a is the predefined limit.

The above considerations lead us to the optimization problem formulation

$$\begin{aligned}
\underset{g,\tau,\theta}{\text{minimize}} \quad & \gamma \frac{\max\{W_{i,\max}(\theta) :\ i = 1,\ldots,d\}}{W_{\text{nom}}} + (1-\gamma)\frac{P_{\max}(g,\tau,\theta)}{P_{\text{nom}}} && \text{(79a)}\\
\text{subject to} \quad & \mathbf{A}\theta \leq \mathbf{b}, && \text{(79b)}\\
& \alpha(g,\tau,\theta) \leq \xi_\alpha, && \text{(79c)}\\
& W_{a,\max}(g,\tau,\theta) \leq \xi_a, && \text{(79d)}\\
& g,\tau \text{ fullfill Proposition 3}, && \text{(79e)}
\end{aligned}$$

where g, τ are control law parameters and θ is the structural parameter set. The parameter $\gamma \in \langle 0, 1\rangle$ allows us to balance the two objectives (75) and (76) according to user-defined priority. Note that the two objectives are to be normalized with respect to nominal values P_{nom} and W_{nom}. The linear inequality constraints (79b) represent physical feasibility limits such as positivity of all parameters and their lower and upper bounds, and possible other specific structural requirements. An example of the latter is a restriction placed on absorber mass m_a to be lower than mass m_p. The stability margin of the overall setup is represented via (79c), which is a nonlinear inequality constraint formed in (77). The nonlinear inequality constraint (79d) poses a limit on maximum of elastic potential energy $W_{a,\max}$ in DR's link, representing the maximum possible load we can redirect from the structure to the absorber. Finally, constraint (79e) ensures full vibration suppression of mass m_s.

Note that variables g and τ and constraint (79e) can be eliminated, using Proposition 3. This is due to the fact that g and τ are determined from structural parameters including those in θ, and thus they are not free. In fact, by choosing the solution (45)–(46) with smallest positive delay, they are uniquely determmined by θ. Therefore, solving the above optimization task can be rephrased as

$$\underset{\theta}{\text{minimize}} \quad \gamma \frac{\max\{W_{i,\max}(\theta) : \ i = 1, \ldots, d\}}{W_{\text{nom}}} + (1-\gamma)\frac{P_{\max}(\theta)}{P_{\text{nom}}} \tag{80a}$$

$$\text{subject to} \quad \mathbf{A}\theta \leq \mathbf{b}, \tag{80b}$$

$$\alpha(\theta) \leq \xi_\alpha, \tag{80c}$$

$$W_{a,\max}(\theta) \leq \xi_a. \tag{80d}$$

Since the objective function (80a), as well as some of the constraint functions, are in general nonconvex and nonsmooth, makes this optimization problem a suitable candidate for an application of the software *GRANSO* [42], which implements a BFGS-SQP method for solving nonsmooth, nonconvex, constrained optimization problems. The application of this method will be demonstrated in the subsequent numerical case study. Before that, we present experimental case study, where we demonstrate the possibility to improve system characteristics towards non-collocated vibration absorption considering two-parameter set for which they can well be mapped and no optimization routine is needed.

4. Structural analysis and optimization of experimental setup

In order to explain the mechanisms by which the optimized parameters influence the optimization objectives, we analyse and optimize parameters of the experimental set-up depicted in Fig. 2. It consists of flexibly linked three masses with configuration $p = 1$, $s = 2$ and $d = 3$, meaning that the absorber is deployed at the mass m_1 and the objective is to suppress vibration of the middle mass m_2. The carts m_1, m_2 and m_3 are attached by industrial ball bearings to the rail fixed on the frame. The absorber m_a is mounted directly on a cart m_1 where it slides on a smaller rail. All carts are flexibly interconnected by springs. A multi-pole magnetic strip is installed on the setup frame to measure the displacement of the

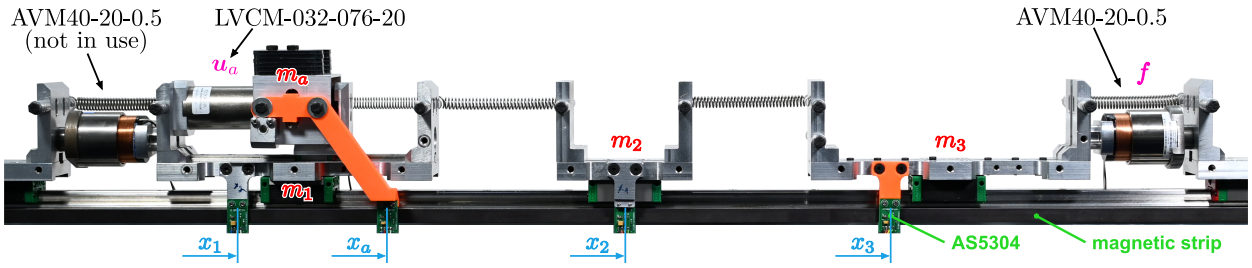

Figure 2: Experimental setup with three flexibly linked carts actuated by the voice coils

carts. The Moticont LVCM-032-076-20 voicecoil is used as the DR to exert the force input $u(t)$, while Akribys AVM40-20-0.5 voicecoil is used to generate the disturbance harmonic force $f(t)$. The control algorithms and instrumentation are implemented in LabVIEW™ 2021 and are executed on the NI compactRIO 9064 industrial control system from National Instruments with a sampling rate of 1 kHz. More detailed description of the setup hardware can be found in [38], [38], and [25], where, in different configurations, it was used for validating different vibration suppression problems.

The harmonic force (1) acting at mass m_3 is characterized by $\bar{f}_d = 2\,\mathrm{N}$ and frequency $\omega = 26.389\,\mathrm{s}^{-1}(4.2\,\mathrm{Hz})$. The nominal parameters of the setup structure are assumed as: $m_1 = 1.49\,\mathrm{kg}$, $m_2 = 0.509\,\mathrm{kg}$, $m_3 = 0.687\,\mathrm{kg}$, $m_a = 0.42\,\mathrm{kg}$, $k_1 = 1001\,\mathrm{Nm}^{-1}$, $k_2 = 749\,\mathrm{Nm}^{-1}$, $k_3 = 711\,\mathrm{Nm}^{-1}$, $k_4 = 950\,\mathrm{Nm}^{-1}$, $k_a = 407\,\mathrm{Nm}^{-1}$, $c_1 = 4.35\,\mathrm{Nsm}^{-1}$, $c_2 = 0.85\,\mathrm{Nsm}^{-1}$, $c_3 = 1.85\,\mathrm{Nsm}^{-1}$, $c_4 = 4.95\,\mathrm{Nsm}^{-1}$, $c_a = 1.8\,\mathrm{Nsm}^{-1}$. Considering the parameters of the decomposed model (21)-(23), we have $\mathbf{A}_R = -\omega^2 m_1 + k_1 + k_2 + \jmath\omega(c_1 + c_2)$, $\mathbf{a}_R = -k_2 - \jmath\omega c_2$, $a_{s,s} = -\omega^2 m_2 + k_2 + k_3 + \jmath\omega(c_2 + c_3)$, $\mathbf{A}_V = -\omega^2 m_3 + k_3 + k_4 + \jmath\omega(c_3 + c_4)$, $\mathbf{a}_V = -k_3 - \jmath\omega c_3$, $\mathbf{D}_a = 1$ and $\mathbf{D}_d = 1$.

Regarding the vector of decisive parameters, we opt for adjusting the masses as the change is easily measurable and can be done by either adding steel plates on the carts or removing them. Before selection of masses to be optimize, the structural analysis is performed. When the vibration of m_2 is fully suppressed, the total force acting on absorber (19) yields

$$\vec{f}_a = -\frac{(-k_3 - c_3\jmath\omega)(-m_1\omega^2 + k_1 + k_2 + (c_1 + c_2)\jmath\omega)}{(-k_2 - c_2\jmath\omega)(-m_3\omega^2 + k_3 + k_4 + (c_3 + c_4)\jmath\omega)}\vec{f}_d. \tag{81}$$

Expressing

$$\vec{x}_1 = \frac{(-k_3 - c_3\jmath\omega)}{(-k_2 - c_2\jmath\omega)(-m_3\omega^2 + k_3 + k_4 + (c_3 + c_4)\jmath\omega)}\vec{f}_d, \tag{82}$$

$$\vec{x}_3 = -\frac{1}{-m_3\omega^2 + k_3 + k_4 + (c_3 + c_4)\jmath\omega}\vec{f}_d. \tag{83}$$

from (24) and (25), respectively, and substituting them to (33) the maxima of the structural potential elastic energies in the links are given as

$$W_{1,max} = \frac{1}{2}k_1\frac{(k_3^2 + c_3^2\omega^2)}{(k_2^2 + c_2^2\omega^2)((-m_3\omega^2 + k_3 + k_4)^2 + (c_3 + c_4)^2\omega^2)}|\vec{f}_d|^2, \tag{84}$$

$$W_{2,max} = \frac{1}{2}k_2\frac{(k_3^2 + c_3^2\omega^2)}{(k_2^2 + c_2^2\omega^2)((-m_3\omega^2 + k_3 + k_4)^2 + (c_3 + c_4)^2\omega^2)}|\vec{f}_d|^2, \tag{85}$$

$$W_{3,max} = \frac{1}{2}k_3\frac{1}{(-m_3\omega^2 + k_3 + k_4)^2 + (c_3 + c_4)^2\omega^2}|\vec{f}_d|^2, \tag{86}$$

$$W_{4,max} = \frac{1}{2}k_4\frac{1}{(-m_3\omega^2 + k_3 + k_4)^2 + (c_3 + c_4)^2\omega^2}|\vec{f}_d|^2. \tag{87}$$

As can be seen, the only mass which affects their value is m_3, which will be considered as the first decisive variable for the analysis. The additional quantity to be observed is the maximum of potential energy at the absorber $W_{a,max}$, given by (58). Expressing

$$\vec{x}_a = \frac{(-k_3 - c_3\jmath\omega)(-m_1\omega^2 + k_1 + k_2 + (c_1 + c_2)\jmath\omega)}{(m_a\omega^2)(-k_2 - c_2\jmath\omega)(-m_3\omega^2 + k_3 + k_4 + (c_3 + c_4)\jmath\omega)}\vec{f}_d, \tag{88}$$

form (42), it is clear that due to dependence of $W_{a,max}$ on $\Delta\vec{x}_{a,p} = \vec{x}_a - \vec{x}_p$, it depends not only at m_3, but also on m_a and m_1. This is also the case for P_{max} given by (64) depending on the product of force

$$\vec{u} = -m_a\omega^2 - (\jmath\omega c_a + k_a)(\vec{x}_p - \vec{x}_a) \tag{89}$$

expressed from (48) and phasor difference of velocities $\jmath\omega(\vec{x}_p - \vec{x}_a)$. Note that full expressions for $W_{a,max}$ and P_{max} are omitted due to their extensive lengths. Due to visualization and demonstration purposes, we select m_a as the second decisive variable, while m_1 is considered as fixed, implying $\theta = [m_a, m_3]^{\mathrm{T}}$. Note also that all the masses play role in evaluating the spectral abscissa (74) under the active delayed feedback (44) with parameters given by (45).

variable	units	lower bound	upper bound	nominal	optimized
θ		θ^{lb}	θ^{ub}	θ^{0}	θ^{*}
m_a	kg	0.220	0.620	0.420	0.520
m_3	kg	0.705	1.205	1.110	0.705

Table 1: Nominal and optimized values of decision variables θ, together with lower and upper bounds.

	Objectives		Inequality constraints		Control law	
setup	$\max_i W_{i,\max}$ [J]	$P_{\max}$ [W]	α [s^{-1}]	$W_{a,\max}$ [J]	g [Nm^{-1}]	τ [s]
nominal	0.00232	0.03129	-0.62415	0.00205	-78.05282	0.03303
optimized	0.00136	0.01855	-0.56855	0.00058	-170.99583	0.01421

Table 2: Comparison of objective function values, and inequality constraints. Results presented for both nominal and optimized parameters.

The analysis of maxima of potential energies $W_{i,max}, i = 1..4$ and $W_{a,max}$, spectral abscissa α, and power maximum P_{max} are shown in Fig. 3. The results were obtained numerically by evaluating the observed quantities at a dense grid and using the plotting functionalities of Matlab. As can be seen in the top-left sub-figure, the dependence of all $W_{i,max}, i = 1..4$ on m_3 is substantial, with maxima achieved for $m_3 = 2.385\,\mathrm{kg}$. Relatively large decay can be observed for both higher and smaller values of m_3 compared to the maximum. In the top-right sub-figure, the spectral abscissa α is visualized by contour plot. The stability boundary (where $\alpha = 0$) is highlighted by thick red line and transferred to the bottom sub-figures, where P_{max} and $W_{a,max}$ are contoured. In all the sub-figures, the admissible parameter ranges according to Table 1 are visualized by red regions. Additional to lower and upper bounds of the masses given by construction constraints, we require m_a to be less then 20% of $m_1 + m_2 + m_3$. The grid points within the red regions correspond to possible mass adjustments, as they only be changed by either adding or removing plates of $0.025\,\mathrm{kg}$ weights. Besides, the nominal and optimized values are highlighted by black circle and star, respectively. As can be seen, both the partial objectives $\max_i W_{i,\max}$ [J] (maximum achieved for $i = 4$) and $P_{\max}$ [W] are minimal for the same mass value set given in Table 1,

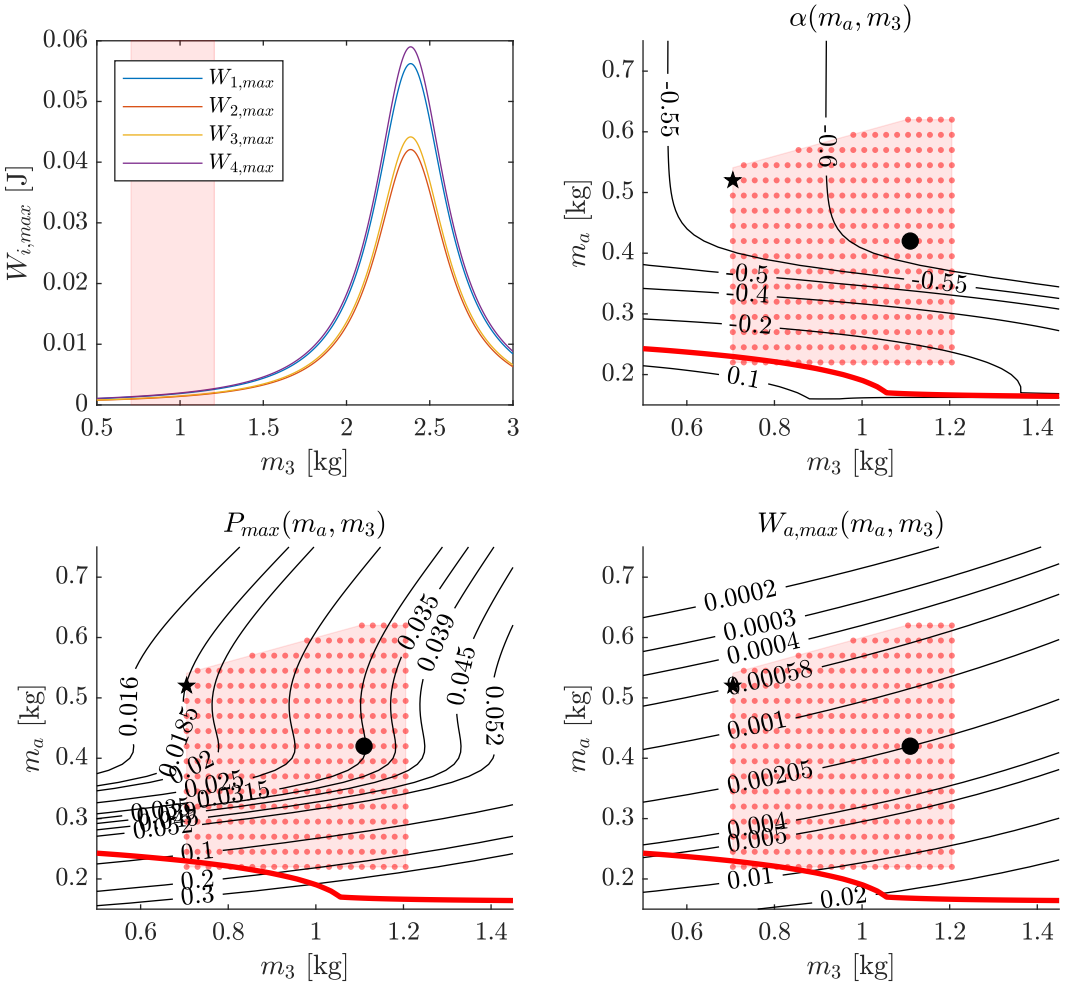

Figure 3: Left column — objectives, maxima of potential elastic energies in links $W_{i,max}$ as a function of m_3 (top), maxima of power as a function of m_3 and m_a. Right column — non linear inequalities as a function of m_3 and m_a, spectral abscissa (top) and maxima of potential elastic energy in absorber link (bottom). Red polygons define structural constraints (linear inequalities), small red dots represent considered grid with 0.025 kg steps. Thick red line represents stability boundary, i.e. $\alpha(m_3, m_a) = 0$. Plane graphs contain marker for nominal (circle) and optimized (star) solutions.

see also Table 2 for comparison of objectives for nominal and optimized parameters and the control feedback gain-delay set. As given in Table 2, the value of $W_{a,max}$ was substantially reduced, while α changed only slightly.

To complete the analysis, the analytical results are confirmed by experimental results

shown in Fig. 4. Note that the passive regime can be seen in the interval $t \in [0, 2.5]$s after which the delayed position feedback of DR is turned on resulting to almost complete vibration suppression at the target mass m_2 after the short-time transient. As can be seen, substantially better performance was achieved with the optimized parameters compared to the nominal parameter set. Thus, the experiment confirms the analytically obtained results.

5. Numerical complex model case study

In order to validate the above proposed optimization based design, within this numerical case study, we consider the system configuration with $d = 5$, $p = 1$, and $s = 3$, i.e., consisting of five masses with the vibration absorber being deployed at the mass m_1, and with the objective to fully suppress vibration of mass m_3. The harmonic force (1) acting at mass m_5 is characterized by $\bar{f}_d = 1\,\mathrm{N}$ and frequency $\omega = 23.248\,\mathrm{s}^{-1}(3.7\,\mathrm{Hz})$. The nominal parameters of the structure are assumed as: $m_i = 1\,\mathrm{kg},\ i = 1, \ldots, 4$, $m_5 = 2\,\mathrm{kg}$, $m_a = 0.5\,\mathrm{kg}$, $k_i = 750\,\mathrm{Nm}^{-1},\ i = 1, \ldots, 5$, $k_a = 700\,\mathrm{Nm}^{-1}$, $c_i = 2\,\mathrm{Nsm}^{-1},\ i = 1, \ldots, 5$, $c_a = 2\,\mathrm{Nsm}^{-1}$.

The optimization problem is considered in the form (80a)–(80d). Contrary to the experimental case study, the parameters to be determined are the stiffness at all the links $k_i,\ i = 1, \ldots, 6$, and a complete DR parameter set $m_a,\ k_a,\ c_a$, while all the other parameters of the system are assumed to be fixed. Thus, the vector of decisive parameters is given by $\theta = [m_a, c_a, k_a, k_1, k_2, k_3, k_4, k_5, k_6]^{\mathrm{T}}$. In Table 3, we refer to θ^{lb} and θ^{ub} as vectors of lower and upper bounds for our decision variables, respectively. Additionally, we denote θ^0 as a vector of *nominal* parameters. For the scaling purposes within the objective function, we assume $W_{\mathrm{nom}}(\theta^0) = \max\{W_{i,\max}(\theta^0) :\ i = 1, \ldots, 6\} = 0.0607\,\mathrm{J}$, $P_{\mathrm{nom}}(\theta^0) = P_{\max}(\theta^0) = 0.0111\,\mathrm{W}$. Additionally, we select $\gamma = 0.5$. Matrices $\mathbf{A} = [\mathbf{I}, -\mathbf{I}]^{\mathrm{T}}$, $\mathbf{b} = [\theta^{\mathrm{ub}}, -\theta^{\mathrm{lb}}]^{\mathrm{T}}$ define the linear inequality constraints from (80b). Stability is guaranteed by imposing a boundary $\xi_\alpha = -0.2\,\mathrm{s}^{-1}$ in (80c), ensuring that the spectral abscissa of the optimized system will not be worse than the nominal one (we refer to Table 4). To enforce inequality constraint (79d), we require the maximum elastic potential energy at the absorber's link to be lower than $\xi_a = 0.01$ J, which can be considered as a rather conservative value.

variable	units	lower bound	upper bound	nominal	optimized
θ		θ^{lb}	θ^{ub}	θ^{0}	θ^{*}
m_a	kg	0.2	2.0	0.5	0.675
c_a	Nsm^{-1}	1.0	10.0	2.0	4.134
k_a	Nm^{-1}	400	2000	700	699.863
k_1	Nm^{-1}	400	2000	750	736.119
k_2	Nm^{-1}	400	2000	750	761.605
k_3	Nm^{-1}	400	2000	750	770.249
k_4	Nm^{-1}	400	2000	750	599.090
k_5	Nm^{-1}	400	2000	750	727.512
k_6	Nm^{-1}	400	2000	750	530.197

Table 3: Nominal and optimized values of decision variables θ, together with lower and upper bounds.

	Objective function ($\gamma = 0.5$)			Inequality constraints		Control law	
setup	J [-]	$\max_i W_{i,\max}$ [J]	$P_{\max}$ [W]	α [s^{-1}]	$W_{a,\max}$ [J]	g [Nm^{-1}]	τ [s]
nominal	**1.0**	0.01115	0.06067	-0.20926	0.00238	-129.96	0.04617
optimized	**0.111**	0.00128	0.00653	-0.22208	0.00005	-368.53	0.01682

Table 4: Comparison of objective function values, inequality constraints and control law parameters for the nominal and optimized parameter settings.

For determining the spectral abscissa, `tds_sa` function from the Matlab *TDS-CONTROL* toolbox [43], [44] is used (with setting: `rhp=-1.2`, `max_size_evp=1200`, `newton_tol=1e-10` and `newton_max_iter=20`). This function implements a spectral discretization method [46] for determining position of the rightmost characteristic roots. The defined optimization task was solved using GRANSO (with setting: `mu0=5.5`, `opt_tol=1e-8`, `rel_tol=0`, `step_tol=1e-12`, `viol_ineq_tol=0`). The required gradients of the objective and constraint functions were approximated by finite differences with spacing `1e-8`.

Optimization task was performed from 100 starting points θ selected randomly respecting the defined upper and lower bounds. Optimization by GRANSO run under MATLAB

R2022a on a workstation with AMD Ryzen 5 2600 (6 physical cores, 3.4 GHz) and 32 GB RAM. The overall solution took 535 minutes. The optimized parameter set is given in Table 3 whereas the values of the criterion and quantities bound by the constrains are given in Table 4. Notice that, interestingly, the decision parameter optimization lead to relatively small adjustments compared to their nominal values. The objective function J was substantially reduced from the normalized value 1.0 to 0.111, projecting the reduction of the maximum of the elastic potential energy $W_{\max}$ from 0.011 15 J to 0.001 28 J, and of DR actuator power $P_{\max}$ from 0.060 67 W to 0.006 53 W. It can also be seen in Table 4 that the spectral abscissa was kept slightly below the α constraint set to $\xi_\alpha = -0.2\,\mathrm{s}^{-1}$. Furthermore, the safety constraint at the DR link $\xi_a = 0.01$ J was satisfied with very large margin as $W_{a,\max}$ was reduced from 0.002 38 J to negligible 0.000 05 J. The DR feedback (44) parameters, were determined by (46) with $k = 0$.

Distributions of the spectra computed by `tds_roots` function of *TDS-CONTROL* toolbox (with the same setting used for `tds_sa`) are shown in Fig. 5 for both the nominal and optimized systems. Due to the involvement of the delay in the applied DR feedback, both systems represented by DDAE (72) (though with different parameters) have infinite number of roots with retarded distribution. From the detail of the rightmost spectrum, the fulfillment of the predefined spectral abscissa constraint can be checked visually.

Results of simulations performed in Matlab-Simulink (solver `ode45`, relative tolerance `1e-6`) for both nominal and optimized systems are shown in the left subfigures of Fig. 6–Fig. 8. Starting from zero initial conditions, first, the transients of the passive regime are shown in the time range $t \in [0, 15]$ s. Subsequently, at $t = 15$ s, the DR's control law (44) is turned on, which results in transients heading towards complete vibration suppression of the target mass m_3, which is (practically) done for $t > 25$ s. In the right sub-figures of Fig. 6–Fig. 8, the amplitudes and relative position of the phasors for the steady-state oscillations are shown, which were obtained analytically for both active and passive regimes (for the passive, see Appendix A).

In Fig. 6, we can see that turning the DR feedback on results in increasing equilibrium motion amplitudes for x_1, x_2, x_4, and x_5 compared to the passive regime. Though, the ampli-

tudes at the active regime for the optimized system are smaller compared to the amplitudes at the passive regime for the nominal system. In Fig. 7, the mass motion is projected to elastic potential energies at the connecting links $W_i,\ i = 1, \ldots, 6$. In the active regime, the maxima of these energies in all the links of the optimized system are substantially reduced compared to the nominal system. Notice also that for the optimized system, when turning the control on, the maxima of energies decrease in the links 2 and 5, while they increase for the links 1, 3, 4 and 6. On the other hand, for the nominal system, the maxima of all the energies increase when comparing passive and active regimes. Note also that $W_{\max}$ from Table 4 corresponds to the link no. 1.

Subsequently, in Fig. 8, all the observed quantities for the DR absorber are shown. Interestingly, for the optimized system, not only the equilibrium amplitude of position x_a, but also the amplitude of the overall force f_a in the absorber's link are slightly smaller for the active regime compared to the passive regime. Both passive and active amplitudes of the optimized system are considerably smaller than the corresponding amplitudes of the nominal system. As regards the control action amplitude, it is only slightly smaller for the optimized system compared to the nominal system. Relatively large difference in favor of the optimized system can be seen in the maxima of targeted elastic potential energies W_a, already for the passive regime. In the active regime, the differences are substantially amplified. Analogous substantial reduction can be observed for the maximum of the needed power, see also Table 4 with the numerical values of $W_{a,\max}, P_{\max}$.

6. Conclusions

A thorough analysis of non-collocated vibration absorption of a system composed of a series of flexibly linked masses and excited by a harmonic disturbance force is performed. Next to the motion amplitudes, the elastic potential energies in the flexible links between the masses are studied with the aim to assess the risk of fatigue across the structure. It is shown that as soon as vibrations at the target mass are fully suppressed, the system can be separated into a vibrating subsystem excited by the disturbance force and the resonating subsystem excited by the force generated by the active vibration absorber. At this stage,

the motion amplitudes and consequently the maxima of the elastic potential energies in the links are uniquely determined by the actuation force amplitude, its frequency and the parameters of the system, and they cannot be changed neither by the absorber parameter adjustment nor by its control feedback. Thus, if the risk of fatigue is to be minimized across the structure, it needs to be done by optimizing the structural parameters of the system.

A preliminary step towards the subsequent optimization based design is a complete parameter assessment of the delayed resonator with position feedback and the stability analysis in terms of determining the spectral abscissa of the whole system. Attention is also paid to determining the power needed for keeping the target mass stopped at the steady-state oscillation stage and to differences between the maxima of potential energies at the passive and active regimes. Taking the findings of the structural analysis into account, the simultaneous structural optimization and control design of the delayed resonator are translated into an optimization problem. Its objective function is selected to balance the maximum from the potential energy set, corresponding to the link most prone to fatigue, and the power needed by the delayed resonator to absorb the vibration at the target. The objective function to be minimized is supplemented by a set of constraints, including stability of the overall system, construction constraints, and safety constraint on the absorber's link.

For validation of the analytical results, two case studies are included. In the first one performed for the experimental setup with three linked masses, the mechanisms by which the optimized parameters influence the optimization objective is explained and experimentally validated. In the numerical case study, the proposed optimization based design is applied to a system consisting of five linked masses. It is demonstrated that the problem can be well solved by the GRANSO optimization tool. The case study documents that the resistance of the system to fatigue as well as the needed power can be substantially reduced by the proposed approach. Further research directions include, the use of more complex feedback laws to either increase stabilization potential or suppress more than one frequency, and the extension to more general structures, studying and compensating the effect of nonlinearities with subsequent experimental validation on a system with more carts. This will also include the involvement of acceleration feedback which will turn the system spectrum posture from

retarded to neutral.

Acknowledgements

This work was supported by the project 24-10301S of the Czech Science Foundation and by the European Union under the project Robotics and advanced industrial production No. CZ.02.01.01/00/22_008/0004590. The third author was supported by the project C14/22/092 of the Internal Funds KU Leuven and the project G092721N of the Research Foundation-Flanders (FWO - Vlaanderen).
The authors thank Professor Nejat Olgac, University of Connecticut, for motivating this work and for a valuable discussion concerning the presented research results.

Appendix A. Characteristics of the passive regime

For consistency, we outline here selected formulas for the steady state of the passive case, mirroring those derived above for the steady-state oscillations of the non-collocated vibration suppression. Assuming $\vec{u} = 0$, and the relation between $\vec{x}_a(t)$ and $\vec{x}_p(t)$ from (48), the force in the absorber's link, in the phasor form, is given by

$$\vec{f}_a = \frac{-m_a\omega^2(\jmath\omega c_a + k_a)}{k_a - m_a\omega^2 + \jmath\omega c_a}\vec{x}_p. \tag{A.1}$$

Using $\vec{x}_p = \mathbf{e}_p^{\mathrm{T}}\vec{\mathbf{x}}$, the system phasor balance by (9) can be turned to

$$\mathbf{P}(\omega)\vec{\mathbf{x}} = \mathbf{B}_d\vec{f}_d, \tag{A.2}$$

where

$$\mathbf{P}(\omega) = \mathbf{A}(\omega) + \mathbf{B}_a\mathbf{e}_p^{\mathrm{T}}\frac{m_a\omega^2(\jmath\omega c_a + k_a)}{k_a - m_a\omega^2 + \jmath\omega c_a}. \tag{A.3}$$

This allows us to express the positions of masses in a linear chain as

$$\vec{x}_i^{\mathrm{p}} = \mathbf{e}_i^{\mathrm{T}}\mathbf{P}^{-1}(\omega)\mathbf{B}_d\vec{f}_d, \tag{A.4}$$

and position of absorber m_a as

$$\vec{x}_a^{\mathrm{p}} = \frac{\jmath\omega c_a + k_a}{k_a - m_a\omega^2 + \jmath\omega c_a}\mathbf{e}_p^{\mathrm{T}}\mathbf{P}^{-1}(\omega)\mathbf{B}_d\vec{f}_d. \tag{A.5}$$

the elastic potential energies are defined as

$$W_i^{\mathrm{p}}(t) = \bar{W}_{i,\mathrm{mean}}^{\mathrm{p}} + \Re\left\{\vec{W}_i^{\mathrm{p}} e^{\jmath 2\omega t}\right\}, \tag{A.6}$$

where, assuming the difference between positions $\Delta\vec{x}_{i,i-1}^{\mathrm{p}} = \vec{x}_i^{\mathrm{p}} - \vec{x}_{i-1}^{\mathrm{p}}$

$$\bar{W}_{i,\mathrm{mean}}^{\mathrm{p}} = \frac{1}{4} k_i \Delta\vec{x}_{i,i-1}^{\mathrm{p}} (\Delta\vec{x}_{i,i-1}^{\mathrm{p}})^*, \tag{A.7}$$

and

$$\vec{W}_i^{\mathrm{p}} = \frac{1}{4} k_i (\Delta\vec{x}_{i,i-1}^{\mathrm{p}})^2. \tag{A.8}$$

The maximal value of (A.6) is then given by

$$W_{i,\max}^{\mathrm{p}} = \frac{1}{2} k_i \left| \left((\mathbf{e}_i^{\mathrm{T}} - \mathbf{e}_{i-1}^{\mathrm{T}}) \mathbf{P}^{-1}(\omega) \mathbf{B}_d \vec{f}_d \right)^2 \right|. \tag{A.9}$$

The potential energies in the links by the base are handled by considering $\mathbf{e}_0 = \mathbf{e}_{d+1} = \mathbf{o}_d$. Finally, the elastic potential energy in the absorber's link is given by

$$W_a^{\mathrm{p}}(t) = \bar{W}_{p,\mathrm{mean}}^{\mathrm{p}} + \Re\left\{\vec{W}_a^{\mathrm{p}} e^{\jmath 2\omega t}\right\}, \tag{A.10}$$

where, assuming the difference between positions $\Delta\vec{x}_{a,p}^{\mathrm{p}} = \vec{x}_a^{\mathrm{p}} - \vec{x}_p^{\mathrm{p}}$,

$$\bar{W}_{a,\mathrm{mean}}^{\mathrm{p}} = \frac{1}{4} k_a (\Delta\vec{x}_{a,p}^{\mathrm{p}})^* \Delta\vec{x}_{a,p}^{\mathrm{p}} \tag{A.11}$$

and

$$\vec{W}_a^{\mathrm{p}} = \frac{1}{4} k_a (\Delta\vec{x}_{a,p}^{\mathrm{p}})^2. \tag{A.12}$$

Maximum of (A.10) can be expressed using (A.4) and (A.5) as

$$W_{a,\max}^{\mathrm{p}} = \frac{1}{2} k_a \left| \left(1 - \frac{\jmath\omega c_a + k_a}{k_a - m_a\omega^2 + \jmath\omega c_a} \right) \mathbf{e}_p^{\mathrm{T}} \mathbf{P}^{-1}(\omega) \mathbf{B}_d \vec{f}_d \right|^2. \tag{A.13}$$

References

[1] D. Richiedei, I. Tamellin, A. Trevisani, Beyond the Tuned Mass Damper: A Comparative Study of Passive Approaches to Vibration Absorption Through Antiresonance Assignment, Archives of Computational Methods in Engineering 29 (1) (2022) 519–544.

[2] L. Yuan, S. Sun, Z. Pan, D. Ding, O. Gienke, W. Li, Mode coupling chatter suppression for robotic machining using semi-active magnetorheological elastomers absorber, Mechanical Systems and Signal Processing 117 (2019) 221–237.

[3] A. Preumont, Vibration Control of Active Structures: An Introduction, 3rd Edition, no. v. 179 in Solid Mechanics and Its Applications, Springer, 2011.

[4] R. Jenkins, N. Olgac, Real-time tuning of delayed resonator-based absorbers for spectral and spatial variations, Journal of Vibration and Acoustics 141 (2), publisher: American Society of Mechanical Engineers Digital Collection (2019).

[5] N. Olgac, R. Jenkins, Actively tuned noncollocated vibration absorption: An unexplored venue in vibration science and a benchmark problem, IEEE Transactions on Control Systems Technology 29 (1) (2021) 294–304.

[6] C. Buhr, M. A. Franchek, R. J. Bernhard, Non-collocated adaptive–passive vibration control, Journal of Sound and Vibration 206 (3) (1997) 371–398.

[7] J. E. Mottershead, Y. M. Ram, Inverse eigenvalue problems in vibration absorption: passive modification and active control, Mechanical systems and signal processing 20 (1) (2006) 5–44.

[8] P. Cha, Imposing nodes at arbitrary locations for general elastic structures during harmonic excitations, Journal of sound and vibration 272 (3-5) (2004) 853–868.

[9] P. D. Cha, Enforcing nodes at required locations in a harmonically excited structure using simple oscillators, Journal of sound and vibration 279 (3-5) (2005) 799–816.

[10] S. Daley, J. Wang, A geometric approach to the design of remotely located vibration control systems, Journal of Sound and Vibration 318 (4-5) (2008) 702–714.

[11] J. Wang, S. Daley, Broad band controller design for remote vibration using a geometric approach, Journal of Sound and Vibration 329 (19) (2010) 3888–3897.

[12] S.-M. Kim, H. Kim, K. Boo, M. J. Brennan, Demonstration of non-collocated vibration control of a flexible manipulator using electrical dynamic absorbers, Smart Materials and Structures 22 (12) (2013) 127001.

[13] S.-M. Kim, J.-E. Oh, A modal filter approach to non-collocated vibration control of structures, Journal of Sound and Vibration 332 (9) (2013) 2207–2221.

[14] D. Richiedei, I. Tamellin, A. Trevisani, Unit-rank output feedback control for antiresonance assignment in lightweight systems, Mechanical Systems and Signal Processing 164 (2022) 108250.

[15] D. Richiedei, I. Tamellin, A. Trevisani, Pole-zero assignment by the receptance method: Multi-input active vibration control, Mechanical Systems and Signal Processing 172 (2022) 108976.

[16] N. Olgac, B. Holm-Hansen, A novel active vibration absorption technique: delayed resonator, Journal of Sound and Vibration 176 (1) (1994) 93–104.

[17] D. Filipović, N. Olgac, Delayed resonator with speed feedback–design and performance analysis, Mechatronics 12 (3) (2002) 393–413.

[18] N. Olgac, H. Elmali, M. Hosek, M. Renzulli, Active vibration control of distributed systems using delayed resonator with acceleration feedback, Journal of Dynamic Systems, Measurement, and Control 119 (3) (1997) 380–389.

[19] M. Hosek, H. Elmali, N. Olgac, A tunable torsional vibration absorber: the centrifugal delayed resonator, Journal of Sound and Vibration 205 (2) (1997) 151–165.

[20] M. Hošek, N. Olgac, A single-step automatic tuning algorithm for the delayed resonator vibration absorber, IEEE/ASME Transactions on Mechatronics 7 (2) (2002) 245–255.

[21] T. Vyhlídal, N. Olgac, V. Kučera, Delayed resonator with acceleration feedback–complete stability analysis by spectral methods and vibration absorber design, Journal of Sound and Vibration 333 (25) (2014) 6781–6795.

[22] D. Pilbauer, T. Vyhlidal, N. Olgac, Delayed resonator with distributed delay in acceleration feedback - design and experimental verification, IEEE/ASME Transactions on Mechatronics 21 (4) (2016) 2120–2131.

[23] T. Vyhlídal, D. Pilbauer, B. Alikoç, W. Michiels, Analysis and design aspects of delayed resonator absorber with position, velocity or acceleration feedback, Journal of Sound and Vibration 459 (2019) 114831.

[24] D. Pilbauer, T. Vyhlídal, W. Michiels, Optimized design of robust resonator with distributed time-delay, Journal of Sound and Vibration 443 (2019) 576–590.

[25] M. Kuře, J. Bušek, I. Boussaada, W. Michiels, S.-I. Niculescu, T. Vyhlídal, Robust delayed resonator with acceleration feedback — design by double root assignment and experimental validation, Journal of Sound and Vibration 576 (2024) 118261.

[26] O. Eris, B. Alikoc, A. F. Ergenc, A new delayed resonator design approach for extended operable frequency range, Journal of Vibration and Acoustics 140 (4) (2018) 041003.

[27] Y. Liu, N. Olgac, L. Cheng, Delayed resonator with multiple distributed delays–considering and optimizing the inherent loop delay, Journal of Sound and Vibration 576 (2024) 118290.

[28] M. Valášek, N. Olgac, Z. Neusser, Real-time tunable single-degree of freedom, multiple-frequency vibration absorber, Mechanical Systems and Signal Processing 133 (2019) 106244.

[29] J. Cai, Y. Liu, Q. Gao, Y. Chen, Spectrum-based stability analysis for fractional-order delayed resonator with order scheduling, Journal of Sound and Vibration 546 (2023) 117440.

[30] Y. Liu, J. Cai, N. Olgac, Q. Gao, A robust delayed resonator construction using amplifying mechanism, Journal of Vibration and Acoustics 145 (1) (2023) 011010.

[31] T. Vyhlídal, W. Michiels, Z. Neusser, J. Bušek, Z. Šika, Analysis and optimized design of an actively

controlled two-dimensional delayed resonator, Mechanical Systems and Signal Processing 178 (2022) 109195.

[32] Z. Šika, T. Vyhlídal, Z. Neusser, Two-dimensional delayed resonator for entire vibration absorption, Journal of Sound and Vibration 500 (2021) 116010.

[33] Z. Šika, J. Krivošej, T. Vyhlídal, Three dimensional delayed resonator of stewart platform type for entire absorption of fully spatial vibration, Journal of Sound and Vibration 571 (2024) 118154.

[34] P. Beneš, J. Gregor, W. Michiels, T. Vyhlídal, Z. Šika, Collocated and non-collocated active spatial absorbers for spatial flexible structures, Mechanics Based Design of Structures and Machines (2024) 1–29.

[35] H. Rivaz, R. Rohling, An active dynamic vibration absorber for a hand-held vibro-elastography probe, Journal of Vibration and Acoustics 129 (1) (2007) 101–112.

[36] D. Filipovic, D. Schroder, Vibration absorption with linear active resonators: Continuous and discrete time design and analysis, Journal of Vibration and Control 5 (5) (1999) 685–708.

[37] D. Filipović, D. Schröder, Control of vibrations in multi-mass systems with locally controlled absorbers, Automatica 37 (2) (2001) 213–220.

[38] H. Silm, M. Kuře, J. Bušek, W. Michiels, T. Vyhlídal, Spectral design and experimental validation of noncollocated vibration suppression by a delayed resonator and time-delay controller, IEEE Transactions on Control Systems Technology 32 (1) (2024) 73–85.

[39] A. Saldanha, W. Michiels, M. Kuře, J. Bušek, T. Vyhlídal, Stability optimization of time-delay systems with zero-location constraints applied to non-collocated vibration suppression, Mechanical Systems and Signal Processing 208 (2024) 110886.

[40] A. Saldanha, W. Michiels, T. Vyhlídal, Non-collocated vibration suppression using delay-based controllers with multiple fixed delays, IFAC-PapersOnLine 56 (2) (2023) 180–185, 22nd IFAC World Congress.

[41] A. Saldanha, A. Peichl, W. Michiels, T. Vyhlídal, Delayed dynamic-feedback controller design for multi-frequency vibration suppression, Preprint of the 18th IFAC Workshop on Time Delay Systems, Udine, Italy (2024).

[42] F. E. Curtis, T. Mitchell, M. L. Overton, A bfgs-sqp method for nonsmooth, nonconvex, constrained optimization and its evaluation using relative minimization profiles, Optimization Methods and Software 32 (1) (2017) 148–181.

[43] P. Appeltans, H. Silm, W. Michiels, Tds-control: A matlab package for the analysis and controller-design of time-delay systems, IFAC-PapersOnLine 55 (16) (2022) 272–277.

[44] P. Appeltans, W. Michiels, Analysis and controller-design of time-delay systems using tds-control. a tutorial and manual, arXiv preprint arXiv:2305.00341 (2023).

[45] M. Kuře, T. Vyhlídal, W. Michiels, I. Boussaada, Spectral design of robust delayed resonator by double-root assignment, IFAC-PapersOnLine 51 (14) (2018) 72–77.

[46] Z. Wu, W. Michiels, Reliably computing all characteristic roots of delay differential equations in a given right half plane using a spectral method, Journal of Computational and Applied Mathematics 236 (9) (2012) 2499–2514.

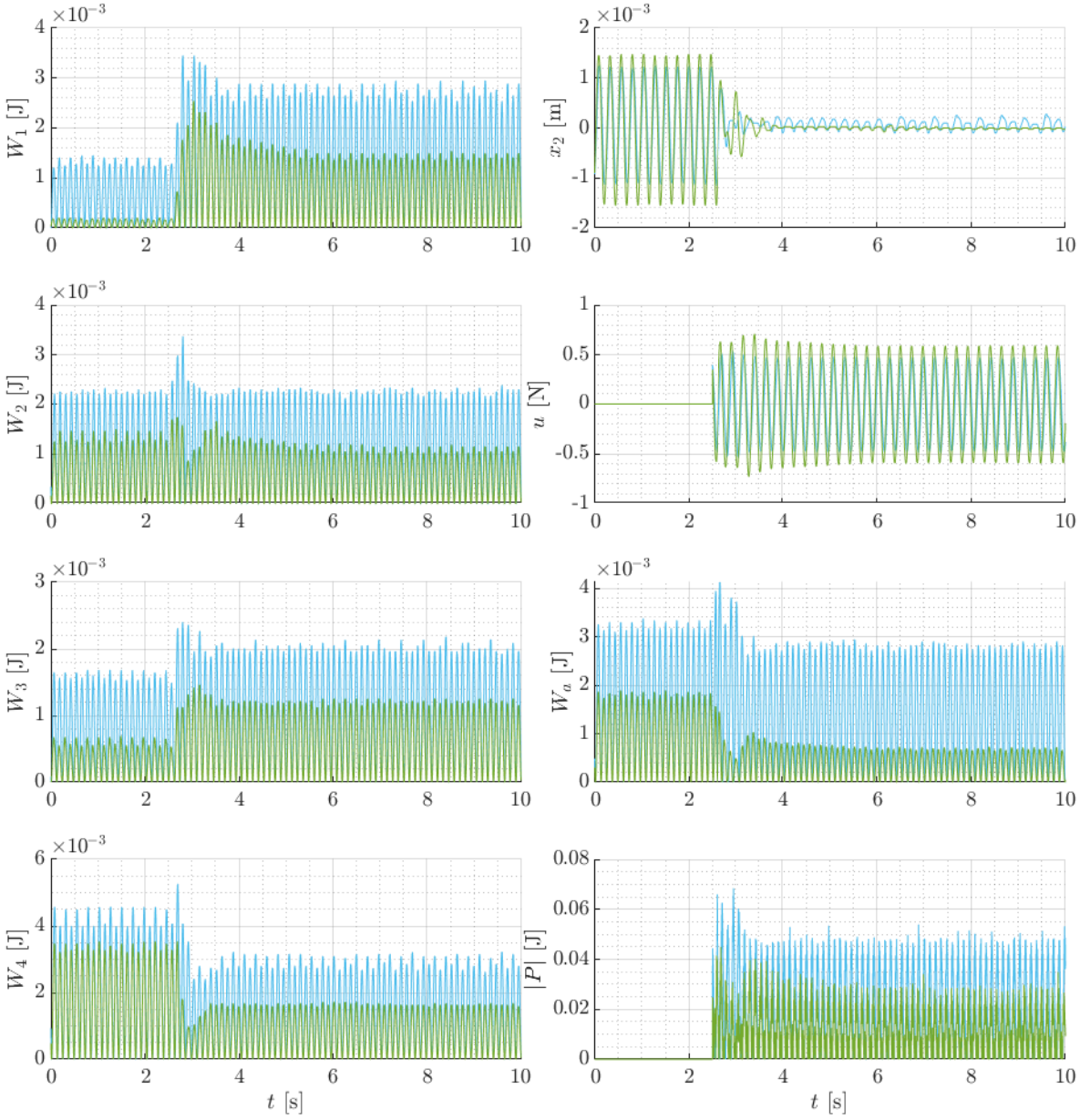

Figure 4: Left — Measured transients of potential elastic energies in links $i = 1, \ldots, 4$ Right — Measured transients (from top to bottom): position of target mass m_2, control force u, potential elastic energy in absorber link W_a, absolute value of power $|P$. For all plots: Nominal parameters (blue) and optimized parameters (green). Passive regime for $t \in [0, 2.5)$ s; active regime $t \in [2.5, 10]$ s.

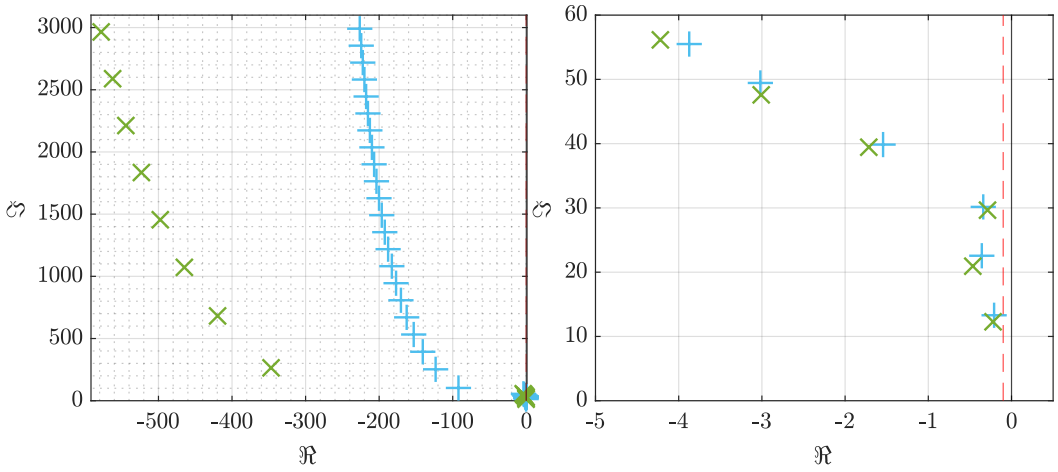

Figure 5: Spectrum distribution of the system with the DR, represented by DDAE (72) with both nominal parameters (blue, +), and optimized parameters (green, x). *Left* — Large scale view; *Right* — Rightmost, stability determining roots with visualized value of the spectral constraint $\xi_\alpha = -0.2$ (red, dashed).

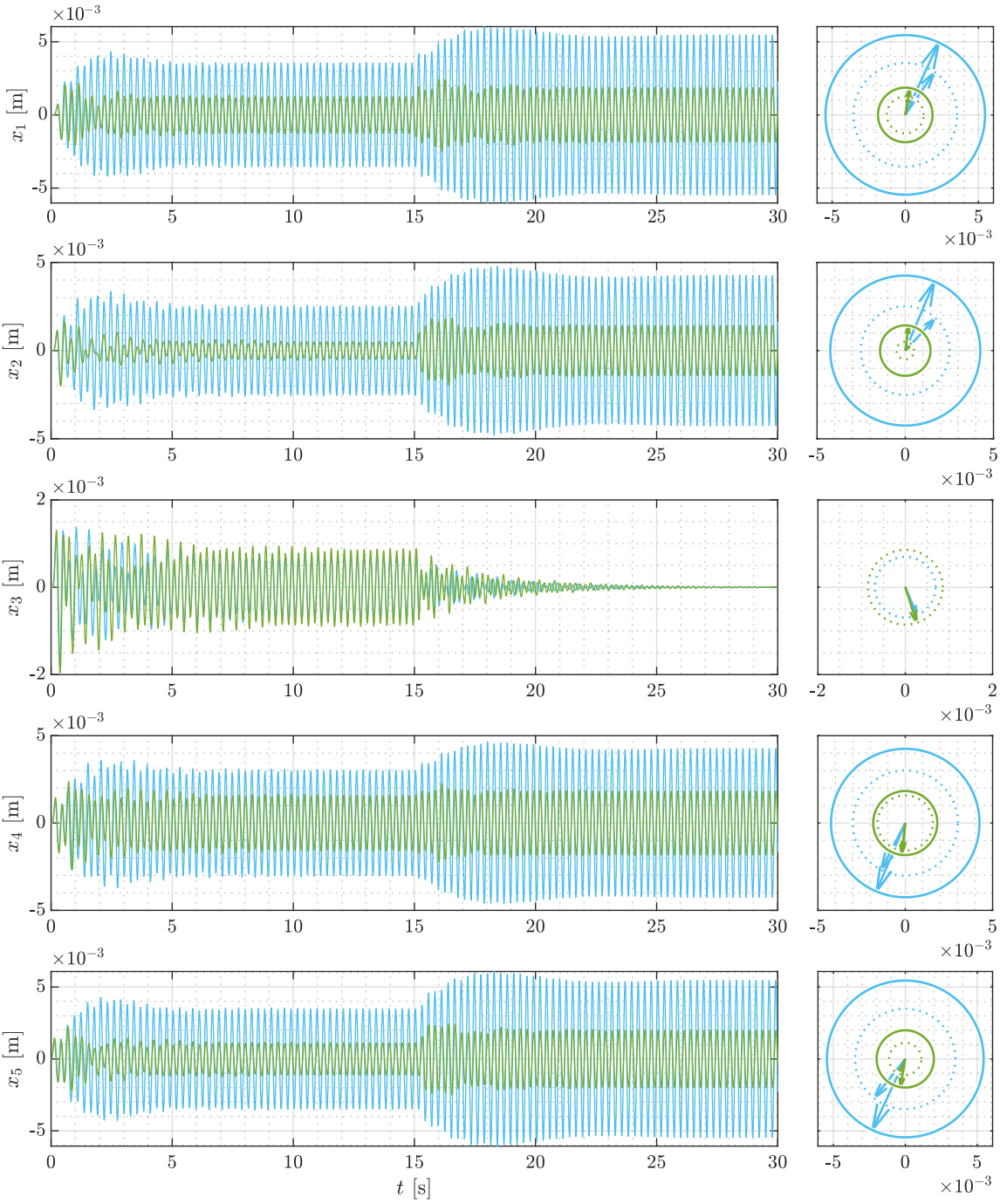

Figure 6: Motion of the masses m_i, $i = 1, \ldots, 5$ for the whole system described by (72) with nominal parameters (blue) and optimized parameters (green). *Left* — Simulated transients from zero initial conditions: passive regime at $t \in [0, 15)$ s; active regime $t \in [15, 30]$ s. *Right* — Equilibrium oscillations in phasor view determined by (A.4) for passive regime (dotted), and either by (24) for x_1, x_2, or by (25) for x_4, x_5 for the active regime (solid).

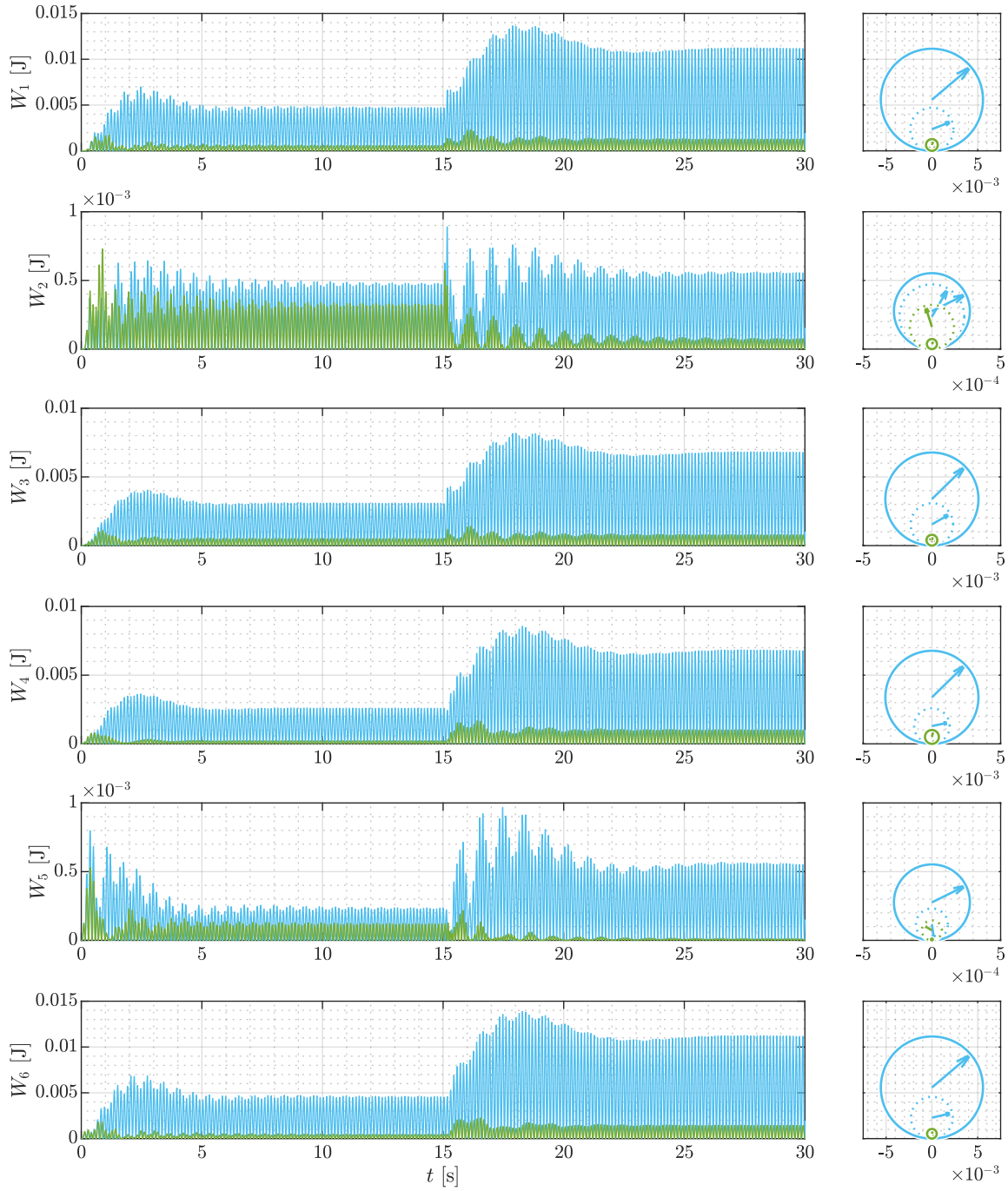

Figure 7: Potential elastic energies in links $i = 1, \ldots, 6$ for the whole system (72) with nominal parameters (blue) and optimized parameters (green). *Left* — Simulated transients from zero initial conditions: passive regime at $t \in [0, 15)$ s; active regime $t \in [15, 30]$ s. *Right* — Equilibrium oscillations in phasor view determined by (A.8) with the center point shifted by time average (A.7) for passive regime (dotted), and by (31) with the center point shifted by (30) for the active regime (solid).

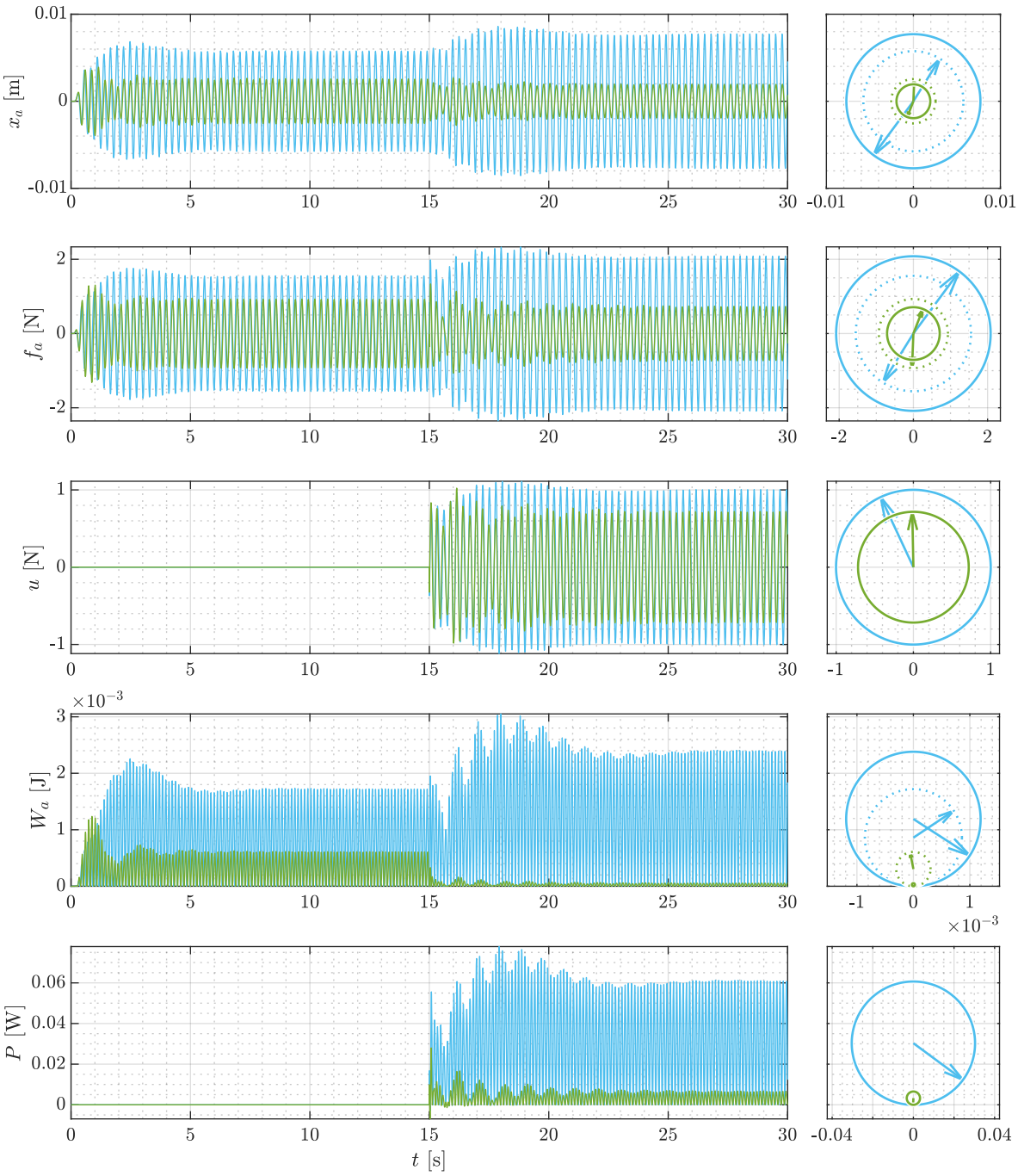

Figure 8: Absorber's characteristics: motion of mass m_a; total force acting on absorber f_a, control force u, elastic potential energy between m_1 and m_a and actuator power P, with nominal parameters (blue) and optimized parameters (green). *Left* — Simulated transients from zero initial conditions: passive regime at $t \in [0, 15)$ s; active regime $t \in [15, 30]$ s. *Right* — Equilibrium oscillations of according quantities in phasor view for both passive regime (dotted, see Appendix A) and active regime (solid, see Section 2.3).